UNIVERSITÀ DEGLI STUDI DI PADOVA

UNIVERSITÁ DEGLI STUDI DI PADOVA

Dipartimento di Ingegneria Industriale DII

Corso di Laurea Magistrale in Energy Engineering

Design and management of an Integrated Thermal Energy Storage System

Relatore: Prof.ssa Anna Stoppato

Correlatore: Prof. Alberto Benato

Simone Peccolo 2053866

Anno Accademico 2022/2023

Abstract

Nowadays our society is experiencing an energy transition, in which renewable energy sources are assuming a newer and more central role in the actual energetic mix. In these scenarios, to boost the decarbonization and the usage of sustainable energy systems, Thermal Energy Storage Systems will play a fundamental role. In fact, given the discontinuous and intermittent behaviour of renewable sources, storage devices allow the mitigation of these effects and the enhancement of the electrical grid. These devices can find room not only for electrical applications, but even in the residential and industrial sectors. In this work, I am going to investigate how to determine the value of the volume of a storage device, part of an Integrated Thermal Energy Storage System, considering different possible management strategies of the system.

Contents

Chapter 1

Introduction

In the last years, important global crisis such as the COVID-19 and the Russia-Ukraine conflict have underlined the problems related to the reliability of fossil fuels and non-renewable sources. The response to these critical situations could reorient the energy geopolitics and speed up the development of renewable energy systems [1]. The pressures on the market, started before, but aggravated by the Russia's invasion of Ukraine, have caused stresses on all the industrial sectors, and in particular on the energetic one. Consequently, the conflict has caused the reduction of the natural gas supply to the Europe and the European Union's sanctions on the import of oil and coal from the Russia are changing the global energy tradings [2]. Thus, these crisis have showed the fragility and the non-reliability of the actual energy system. The governments are studying long-term solutions in order to speed up the structural changes towards a greater penetration of the renewable energy sources in their actual energetic mix. In this optic, the possibility to store the energy produced by renewable sources, can assume a central role to guarantee the energetic stability of a country. Furthermore, the implementation of energy storages in the energy systems can lead to an improvement of the flexibility of the supply of electricity [2].

Besides the fragility of the actual energetic mix, another aspect that pushes towards a higher use of the renewable sources is the increase, at global level, of the CO_2 and greenhouse gas emissions. Being these a leading cause of the climate change,

practical actions able to change the management of natural sources and the energy are required [3]. Anyway, the increase of renewable sources in the actual energetic mix leads to problems related to the non-constant and unpredictable behaviour of these sources for the stability of the entire electrical sector, with a special focus on the electrical grid. In fact, the intermittent generation causes disturbs in the networks and additional stresses with respect to conventional generation systems. The possibility to couple these intermittent sources with energy storage technologies may enhance, support and improve the adaption of the grids in terms of reliability and efficiency [4]. The development of renewable energy systems requires efficient management systems, able to optimize the performances of the entire energy network through the implementation of modern techniques such as the artificial intelligence and the coupling between renewable sources and energy storages [5]. Moreover, it is clear that the need of energy storage devices is increasing with the increase of renewable energy penetration [6]: in the following Figure 1, we can see the forecast of global cumulative energy storages installations, that are expected to increase a lot in the next decades.

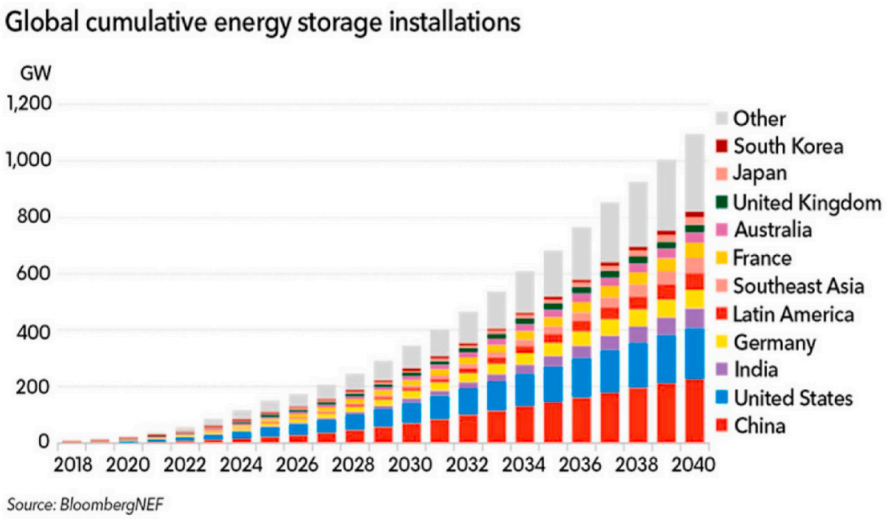

Figure 1.1: Prediction of the installments of energy storages until 2040 [6].

Therefore, we can understand that the energy storage technologies will assume a central role in the future strategies to manage renewable energy sources in the proper way. In this optic, there is an urgent need to investigate and develop new solutions and strategies in the energy storage sector.

In particular, in this work we are going to investigate the thermal energy storage systems, with a special attention to the Integrated Thermal Energy Storage Systems. The aim is to understand which could be a possible way to determine the volume of the storage device and its behaviour always taking into consideration the other devices that constitute the Integrated Thermal Energy Storage Systems.

Chapter 2

Literature review

Before proceeding with the analysis of the work, it is important to start with a brief literature review to introduce and analyse the main concepts of this work. According to this, we are going to analyze the concepts of energy storage, investigating the various solutions and technologies proposed in the past years. Another aspect regards the so-called Carnot batteries, among which we can find the central role of the Integrated Thermal Energy Storage Systems. Lastly, to investigate possible management strategies of the storage system, the concept of Virtual Power Plant is introduced and studied.

2.1 Energy storage systems technologies

As said, one of the main challenges we are facing in the energy sector regards the necessity to store energy in form of electricity or heat, in order to reduce the consumption of fossil fuels and consequently the emissions of pollutants and carbon dioxide. Moreover, the possibility to store energy in this forms can help in the usage of variable renewable energy sources, and improve their penetration in the actual energetic mix of our countries. Dealing with the energy storage technologies, it is important to define, first of all, the concept of energy storage. According to Benato and Stoppato [7], an energy storage is a device or a system in which the energy

can be stored in a certain form. In a second moment, this energy can be extracted to perform some useful operations. The process of storing can be subdivided into three main phases: charging, storing and discharging. During the charging phase the energy enters the storage device. Then, during the second phase, the energy remains inside the storage system and during the discharging phase it is released.

Over the years, various classifications of storage systems have been proposed: a possible way, is the one proposed by Aneke and Wang [8]. This classification derives from the concept of primary and secondary energy forms: the first group includes all that forms of energy that are not subjected to any transformation or conversion process, while the energy forms that are the product of a process of transformation are considered secondary energy. In the first group we can find sources such as coal, gasoline and natural gas, and in the second one we have electricity, thermal energy, hydrogen and so on. The energy derived from the sun, wind or the sea can be stored only after a transformation process; sources such as coal, fuels and hydrocarbons can be stored directly in their own form. Consequently, a possible way to classify the storage system is between primary and secondary ones.

A different classification, again presented in [8], is the one based on the possibility to divide the storage technologies into electrical and thermal ones. When the electricity is transformed into another form, stocked and during the discharge phase is converted back into electricity, the system is defined as electrical storage system, whereas if the energy is converted back into thermal energy the storage process is called thermal energy storage. Electrical energy storages can be classified as mechanical, chemical, electrochemical and superconducting magnetic storage. Thermal energy storages comprehends sensible heat storage, latent heat storage and thermochemical heat storage.

It is important to highlight that all forms of energy can be stored through appropriate technology; each storage technology is characterized by a certain operating range and can be integrated at different levels of the electrical system. Moreover, the various technologies are characterized by different advantages and disadvan-

tages, with different scale of applicability. Anyway, as emphasized in [7], none of the available technologies in the storage field are able to meet all the needs of an ideal storage system. Consequently, to better familiarize with the various solutions proposed over the years, it is convenient to briefly introduce the most mature and available technologies.

As highlighted by Benato and Stoppato [7] and Aneke and Wand [8], among the most mature technologies for energy storing, we can found the pumped hydro storage systems. Firstly developed in Italy and Switzerland and later in the United States of America, these systems use gravity to move the water from a reservoir placed at a low level to another one in a higher position. A typical plant layout consists of an upper and a lower reservoirs, a pump and a turbine [9], as we can see in Figure 2.1. The off-peak electric power is derived from the grid and used to feed the electric motor which drives the pump. In this way, the water is pumped from the lower to the upper reservoir and stored in this second site. During high demand hours, the water is released from the upper to the lower reservoir through a turbine, mechanically coupled with an electric generator which transforms the mechanical energy into electrical one and injects it again in the electric grid. The major drawbacks of this technology regard the availability of water and an adequate morphology of the installment site: in particular, a sufficiently high altitude difference between the two water basins is required. This storage technology covers around 99% of the world large-scale energy storage installations, is characterized by a very low energy density (0.5-1.5 Wh/l or 0.5-1.5 Wh/kg) and low self-discharge problem (0.005-0.02 %/day). Moreover, the price per unit of power installed is acceptable (5-100 $/kWh). This storage systems are fast-responding, providing reliable power in a short time (generally, around one minute). Defining the round-trip efficiency ad the ratio between the produced energy during the discharge phase and the one absorbed in the charge one, for this technology the value is high (65-87 %) [7].

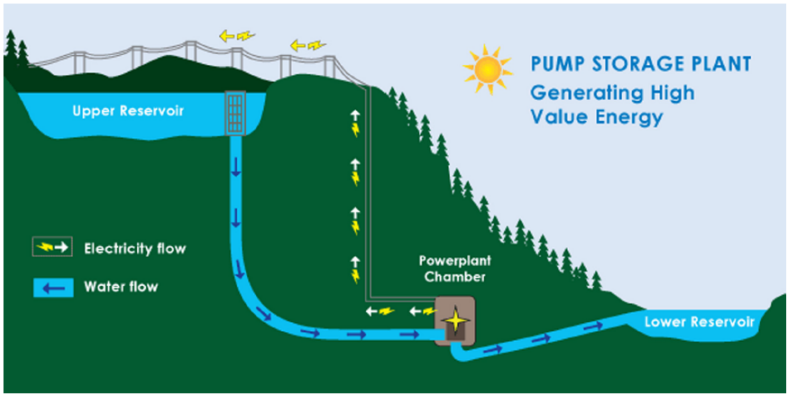

Figure 2.1: Scheme of a pumped hydro energy storage [8]

The second commercially available technology is the so-called compressed air energy storage [7] [10]. In the following Figure 2.2, it is reported a schematic view of a compressed air energy storage system. When the power demanded by the users or the grid is low, the excess in the generation capacity is used to compress the air and subsequently store it in an underground cavern or in man-made devices, able to contain the compressed air. During the high peak demand hours, the stocked and pressurized air is taken from the storage. Once heated up, usually through the use of natural gas, the air is expanded in a turbine. The turbine is mechanically coupled with an electric generator: through this device the potential energy of the pressurized air is converted back into electricity an it is injected back into the electrical grid. Anyway, due to the usage of fossil fuels in the heating of the pressurized air, the environmental impact of this technology must be properly taken into account. Recently, in order to mitigate this negative aspect, other plant configurations were studied with a special attention to the possibility to recover heat from the process. Similarly to the case of pumped hydro energy storage, the compressed air energy technology suffers of the morphological constrains and requires the proper installation site. The round-trip efficiency is in the range 40–89%, the energy density and the price per stored energy unit are of 3–12 Wh/l (or 30–60 Wh/kg) and 2–50 $/kWh, respectively. The capital cost is estimated in the range 400–800 $/kW, while the power rating, the storage capacity and the lifetime are 5–300 MW, higher than

1000 MWh and 20–60 years, respectively.

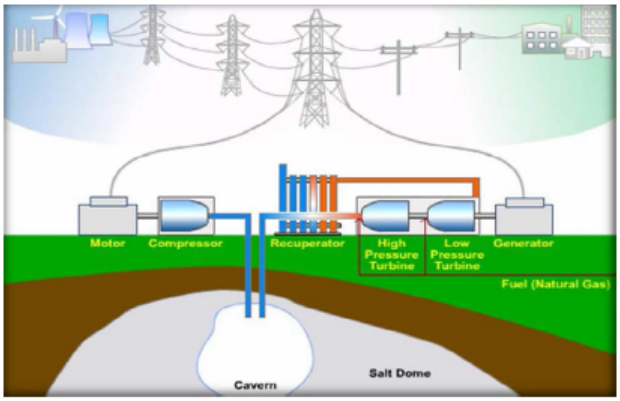

Figure 2.2: Scheme of compressed air energy storage technology [7]

Another recent technology developed for large-scale storage systems is represented by the flow batteries. The functioning is similar to the one of conventional batteries: the ions flow from the negative and the positive electrodes during charging and delivery phases respectively, through a special selective membrane. The negative aspects of this technology regard the poor lifetime and the high capital costs, as reported in [7].

Downstream these considerations, we can clearly understand the urgent need of developing new large-scale storage technologies and systems that do not suffer of geographical constrains and limitations, high investment costs and need of fossil fuels. Many other in-developing technologies were studied such as the ones based on the gravity, the liquid-air energy storage and the hydrogen energy storage.

Generally, gravity energy storage systems exploits the movement of elements such as pistons, wagons or gravel buckets, due to the gravity to generate electricity. Of course, there is the need of a sufficiently high difference in altitude. The moving elements are sent to a higher level during the hours of surplus in the production, storing the energy in form of potential energy, that is recovered in a second moment through the movement of the elements from a higher to a lover position.

The aim of liquefied air energy storage system is to compress the air and store it in liquid form inside some tank or vessels, insulated towards the external environment. During the discharging phase, the air is heated up and the pressure increased. The air is then expanded in a turbine and the energy is recovered through the usage of an electric generator.

Another in-developing technology is based on the possibility to store energy in form of hydrogen: during the charging phase, exploiting the electrolysis process it is possible to produce hydrogen from the water. Hydrogen is then stored in gaseous or liquid form. Once the requirement of energy is increased, the hydrogen is used in a fuel cell of in a gas turbine to produce useful energy.

The last in-developing technology is the pumped thermal electricity storage (PTES), also called pumped heat energy storage. This last technology is based on a high temperature heat pump cycle, which transforms the off-peak electricity into thermal energy and stores it inside man-made vessels (hot and cold). According to Gil et al. [11] and [12], the heat can be stored as sensible or latent heat. During delivery, a thermal engine cycle is used to convert the stored thermal energy into electricity. Usually, the working fluid is a gaseous medium, such as argon or air, while the electricity is stored as sensible heat, exploiting cheap and reliable materials like concrete, common minerals or gravel. Compared to other technologies, it is characterized by higher energy density (110–170 Wh/l or 50–140 Wh/kg), low self-discharge rate (1%/day), no geographical and morphological limitations and small occupation of soil. Since the materials and the fluids used are cheap, the installment costs are low (600 $/kW and 60$/kWh). Moreover, it does not suffer of low cycle life (like the flow batteries). Lifetime and round-trip efficiencies are very good (respectively, 25-30 years and 70-80%). For these reasons, and considering that the storage capacity can be really high (between 0.5-10 MW or larger or 0.5-60 MWh or larger), we can understand that this is one of the most promising large-scale energy storage technologies [7].

Resuming, pumped hydro storage is the most widespread large-scale energy stor-

age technology while compressed air energy storage can be considered its actual most important competitor while flow batteries can become a useful way of storing large quantity of energy only in future. Unfortunately, pumped hydro storage systems require a particular morphology of the installation site, a sufficiently high water fall and a regular water flow rate. Similarly, compressed air energy storages require a particular morphology of the installation site and a natural gas stream. Flow batteries do not require particular morphology of the installation site and are characterised by a high energy density compared to the other two technologies mentioned above, but they suffer of low lifetime. Therefore, to properly match the demand in an electric system composed by a large number of variable and intermittent power plants fed by wind and solar, there is the need of developing large-scale energy storages which do not suffer of geographical constrains, low lifetime or round-trip efficiency. In this scenario, Pumped Thermal Electricity Storage constitutes a valid and really promising alternative to the other technologies [7].

2.1.1 Pumped Thermal Energy Storage Systems

In this work, particularly important are PTES systems, that can be seen and described as Carnot batteries: these are devices in which the electrical energy is stored in form of thermal energy and is lately recovered into electricity during the discharging phase. Carnot batteries are made up of pumps, compressors, expanders, turbines and heat exchangers. Dumont et al. [13] define in a more precise way the concept of Carnot batteries: they are systems primarily used to store electric energy, in which the electric energy (considered as an input) is used to establish a temperature difference between two environments, named low temperature (LT) and high temperature (HT) reservoirs. Consequently, the storage system is charged, converting electrical energy in form of heat (HP). During the discharge phase, the thermal energy is discharged by allowing the heat flowing from the HT to the LT reservoir. The heat flow is used to powers a heat engine (HE) which converts the heat itself into work and discharges the residual heat into the LT reservoir. In this way, a

fraction of the electric input, required during the charging phase, is recovered. To improve the performances of the system, solutions with several heat sources can be adopted. The schematic representation of the concept of Carnot battery is reported in the following Figure 2.3: in particular, the high and low temperature regions are highlighted, also showing the possible integration of thermal energy. Moreover, it is possible to see the electricity flows, required during both the charging and the discharging processes.

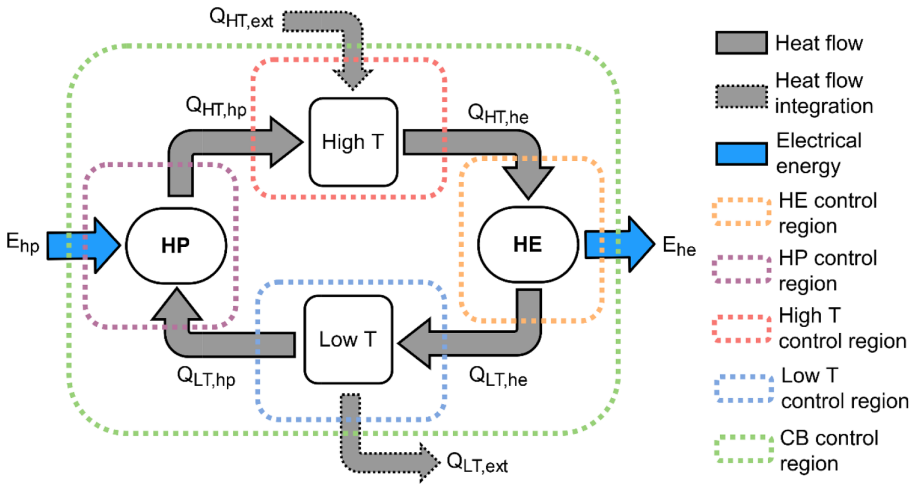

Figure 2.3: Definition of a Carnot battery [8]

Thus, among the Carnot batteries, we can find the concept of Pumped Thermal Energy Storage system that is one of the central aspects of this work. As we have previously seen, through the usage of this systems we have the possibility to store the electricity in form of heat (sensible or latent). Despite the way of storing the heat, in a PTES system the electricity is converted into heat using a high temperature heat pump and stored into man-made tanks or vessels. Then, the heat is converted back into electricity through heat engines.

A possible classification of pumped thermal energy storage systems, can be the one based on the thermodynamic cycle and the working fluid used [7]:

- Closed or reversible Brayton cycle;
- Transcritical Organic Rankine cycle with carbon dioxide as working fluid;
- Compressed Heat Energy Storage system.

The first plant arrangement, uses a single phase gas such as argon or air and is characterized by the presence of two reservoirs, the high pressure and the low pressure ones. The electricity is stored in form of sensible heat. Transcritical ORC are equipped with ice and pressurized water storage tanks. Compressed Heat Energy Storage exploits the evaporation of low pressure water through a heat pump or a refrigerating cycle. After the compression phase, the steam released its energy in a reservoir and it is condensed and cooled down. In the delivery period, the heat released by the storage system is used to generate steam to be used in a steam turbine.

The Brayton PTES for large-scale applications was firstly proposed by Desrues et al. [14].

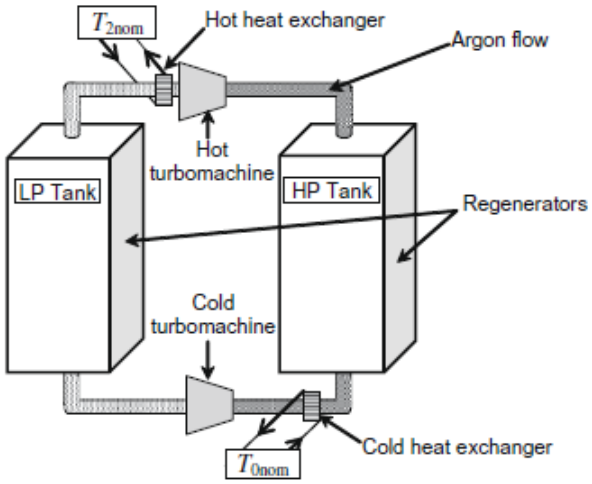

Figure 2.4: Schematic representation of the storage principle [14]

During the charging phase the system works as a heat pump, transforming the electricity into thermal energy, that is then stored inside two artificial tanks. A thermal engine is used for the discharging phase, to convert again the thermal energy into electricity.The turbomachines used (two pairs of a compressor and a turbine), allow the circulation of a gas in the tanks, following a closed thermodynamic Brayton cycle. The heat is stored in a sensible form and the working fluid used is argon. It is important to observe the presence of two different heat exchangers in the configuration, as reported in Figure 2.4.

During the charging phase, the gas moves from the high pressure to the low pressure tank. The high pressure tank is gradually heated up, while the low pressure one is cooled. In the discharging period, the gas follows a heat engine cycle. During this phase, the low pressure tank gradually increases its temperature. Both the charging and the discharging periods are considered completed when the temperature of the gas at the outlet of the reservoirs reaches a predefined value taken as tolerance.

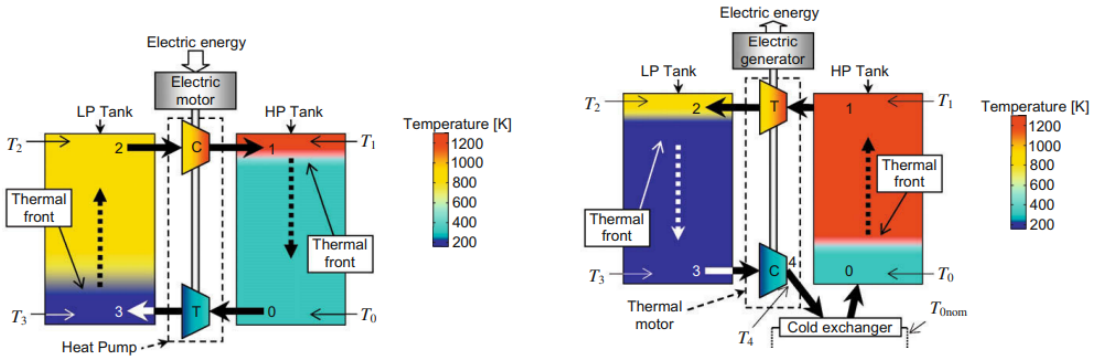

(a) *Charging phase* (b) *Discharging phase*

Figure 2.5: Description of the charge and the discharge of the storage system [14].

More recently, a new configuration was proposed by Benato [15] and Benato and Stoppato [16]. The system consists of a high pressure tank, a low pressure tank,

two turbomachines (a compressor and a turbine, mechanically coupled), an electric motor, an electric heater and a heat exchanger. The electric energy is stored in the form of sensible heat, and the working fluid is air. The choice of air as working fluid, is related to its non toxicity and flammability, its abundance and safety.

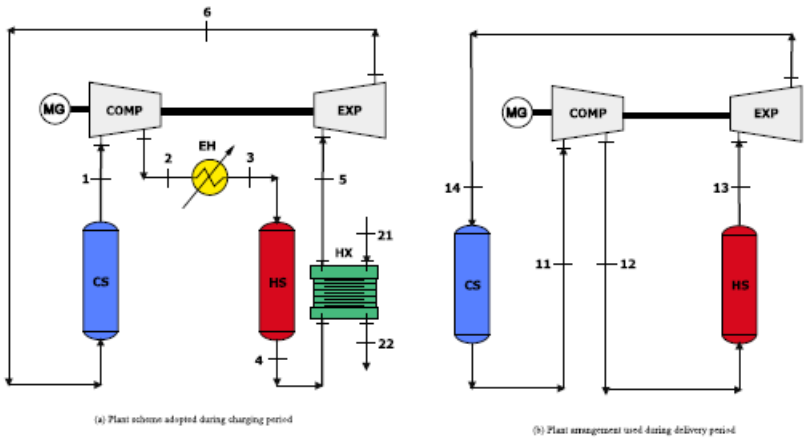

Figure 2.6: Schemes of the PTES system, as proposed in [15].

As we can see in Figure 2.6, during the charging phase the air enters in the compressor, proceeds through the electric heater. Then, entering in the storage tank it exchanges heat with the storage material and proceeds through the heat exchanger to have a suitable temperature value before the inlet of the turbine. After the turbine, the air flows in the cold storage tank. The electric heater is located after the compressor in order to maintain constant the temperature of the air at the inlet of the hot storage tank. Moreover, with this configuration, the maximum temperature of the cycle is reached in correspondence of the inlet of the tank; with previous configurations, in which the electric heater is located before the compressor, the maximum temperature of the cycle is reached at its outlet with the consequent increase of the pressure ratio and the cost of the device. Thus, with the new configuration proposed, it is possible to adopt lower pressure ratio, high maximum temperature of the cycle and acceptable cots and heat transfer area. Moreover, in this new configuration

only one heat exchanger is required, with consequent reduction of the costs and the complexity of the system.

During the delivery phase, the air that leaves the compressor, enters into the HS tank where is heated up. Then, the air is expanded using the turbine and injected into the cold tank, in which its is cooled. In this phase the heat exchangeres are not required, with consequent reduction of the costs of the plant.

The second configuration related to the pumped thermal energy storage systems has been proposed by Mercangöz et al. [17]. In this work, the authors observed that the typical arrangement of PTES systems requires large storages. Thus, they proposed a new configuration in which a transcritical CO_2 cycle is adopted, with the scope of increasing the efficiency of the plant. Other works were proposed, like the ones of Morandin et al. [18] [19], in which the authors analysed different CO_2 transcritical cycle in order to study their optimization. The general scheme of these kind of plant comprises a hot and a cold side. During the charging phase, the heat pump cycle is used to heat the water inside the tanks at a high temperature level. During the discharge, the hot water is used to feed the thermal engine. The usage of carbon dioxide allows to obtain a better match between the thermal profiles of the cold and the hot storages.

The last modification of PTES systems is the one called compressed heat energy storage, proposed by Steinmann [20]. The system proposed is based on the conventional steam Rankine cycle. During the charge, the water at low pressure is evaporated using the heat coming from a low temperature source such as a heat pump or a refrigeration cycle. After the compression process, the high pressure steam releases its energy in a thermal storage reservoir. Then, in this storage, the steam is condensed and the condensate is cooled down to the saturation temperature of the evaporation process. During the discharging process, the heat released by the storage system is used to generate steam used to feed the steam turbine. After the expansion process, the steam is condensed.

Therefore, for large-scale energy storage purposes, the closed Brayton cycle or

reversible Brayton cycle is the only plant arrangement that can be adopted. It is based on a high temperature heat pump cycle, which transforms electrical energy into thermal energy and stores it inside thermal reservoirs, followed by a thermal engine cycle, which transforms the stored thermal energy back into electrical energy. The main components are a compressor, an expander and two thermal stores: one hot and one cold [16].

Downstream these considerations, we can clearly understand that a crucial and central element of Pumped Thermal Energy Storage Systems is represented by the thermal energy storage itself [13]. Different solutions are available and presents different characteristics:

- Sensible thermal energy storage: the heat is stored or rejected exploiting the increase or the decrease of the temperature. The materials used are present always in a single phase, typically solid or liquid. Different materials can be valid for this type of storage, such as water (liquid) or rocks (solid): generally the materials are cheap and safe and represent a simple way to store energy [7]. With the Brayton configuration of the Carnot batteries, the packed bed sensible heat storage configuration is adopted: in this way high temperatures can be reached and there is a direct heat transfer between the storage material and the working fluid. In this way, a higher efficiency of the system can be obtained. However, the use of packed bed presents some drawbacks, like the high pressure drops and non-negligible thermal stresses. Another issue regards the difficulty in performing proper measurements of the temperature level of the storage system.

- Latent thermal energy storage: the heat is stored in materials that undergo through a phase change during charging or discharging phase. The transitions between two phases (generally solid to liquid or vice versa), occurs at an almost constant temperature and thus a better match between temperature profiles can be obtained. Mostly, the phase-change materials used in this technology,

are molten salts, metals (but they often are corrosive) or polymers (but the temperature range seems to be not suitable for Carnot batteries [13]).

- Liquid air energy storage: this technology exploits the liquefaction of air to store the energy. In this way we can have a compact and cheap solution. Anyway, according to Dumont et al., this technology reaches lower efficiencies with respect to other solutions [13].

- Termochemical energy storage: the process of storing and releasing heat through chemical reaction mechanisms is the underlying principle behind thermochemical energy storage. These materials present good energy storage capacity and energy density, but are not available on a highly commercial scale [13].

- Hybrid thermal energy storage: this methodology represents a new emerging method for a large-scale energy storage system, that combines both sensible and latent thermal energy storages.

For Carnot batteries based on the Brayton cycles, for which high temperature levels are expected, the packed bed made with rocks or molten salts seems to be the most suitable materials. For Carnot batteries related to the Rankine cycle with lower temperatures it is possible to use water; oil, instead, is more suitable with higher temperatures. For both the applications phase change materials can be adopted [13].

2.2 Integrated thermal energy storage system

Seen the urgent need of develop and install new large-scale energy storage systems, Benato and Stoppato proposed a new storage unit that uses air as working fluid and stores electricity under the form of sensible heat [21]. This new energy storage system is called *Integrated Thermal Energy Storage System* (IT-ESS), and assumes a central role in the work here presented. Devices that constitute existing fossil fuel thermal power plants such as gas turbines, electric generators, step-up transformers, transmission lines, and so on, can be used to build I-ESS plants. In this way, the installation of the storage unit does not result in additional overcapacity, helps to repower underutilised unit and guarantees to satisfy the pressing need of network flexibility in terms of load levelling, aspect that is assuming a central role for the proper penetration of renewable sources in the energy sector.

Basically, when the production from renewable sources, such as solar or wind, is high and, at the same time, the energy required by the users is low, the surplus of electricity is converted into heat through an electric heater and is stored in the high temperature sensible heat storage unit consisting of a packed bed. During peak hours, in which the energy demanded by the users is high, a modified air bottoming cycle (ABC) unit is used to generates electricity exploiting the previously-stored thermal energy. The heat transfer fluid used is air and the plant works, during the charging phase, as an open cycle and consists of a high pressure and temperature storage tank, a fan, an electric heater, an electric motor and a heat exchanger. During the discharge, the systems consists of an air compressor and turbine, a heat exchanger, a high temperature sensible heat thermal energy storage and an electric generator. Typically, an ABC cycle is a gas turbine, in which the combustion chamber is replaced by a heat exchanger. This device allows to recover the exhaust heat from a topping cycle, and represents a valid alternative to conventional steam Rankine cycle or organic ones, due to its compactness and low weight.

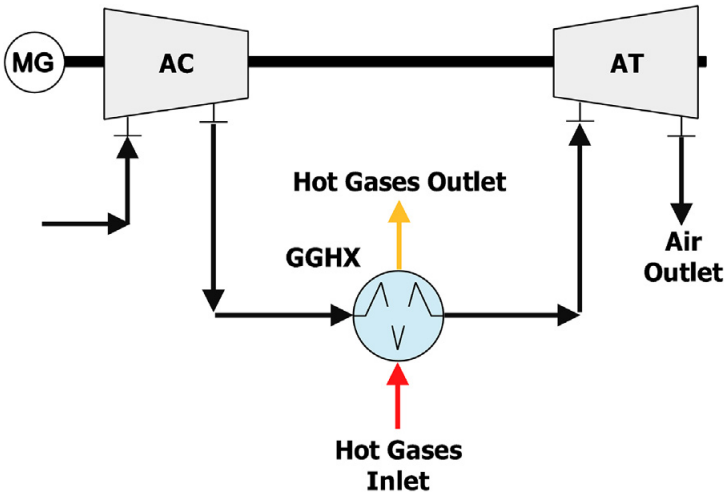

Figure 2.7: ABC in its basic configuration [21].

In the work of Benato and Stoppato [21], the heat exchanger is substituted with the high temperature sensible heat thermal energy storage: in this way, we can clearly understand that the revamping of an already-existing thermal plant based on a gas turbine can be easily performed. More in detail, the system proposed consists of a high pressure and temperature tank (HS), a fan (FAN), an electric heater (EH), a compressor (COMP) and a turbine (EXP) mechanically coupled, an electric motor (MG) and a heat exchanger (HX). During the charging phase (figure 2.8a), the fan forces the air through the heat exchanger. Then, the air is heated up thanks to the electric heater and it proceeds inside the storage tank. After that, the air proceeds through the heat exchanger in which transfers part of the residual heat to the air at the inlet.

During the charging, the material of the storage unit slowly increases its temperature. Thus, the air exiting the tank increases its temperature too. Consequently, to improve the performances of the overall system, it is convenient to install a heat exchanger to recover part of the heat of the air at the outlet of the tank. Moreover, the use of an electric heater allows to maintain always the temperature at the inlet of the storage tank at the maximum value of the cycle. This is an important aspect introduced by the authors in [21]: in fact, in other plant configurations the maximum

temperature is reached at the outlet of the compressor, where the temperature of the working fluid is increased due to the irreversibilities in the compression process [22]. Higher temperature corresponds to a higher pressure at the discharge and a higher pressure ratio. So, the costs of the compressors are higher too. To overcome this problem, the configuration proposed by the authors can be adopted: in this way the pressure ratio remains constant during the charging phase.

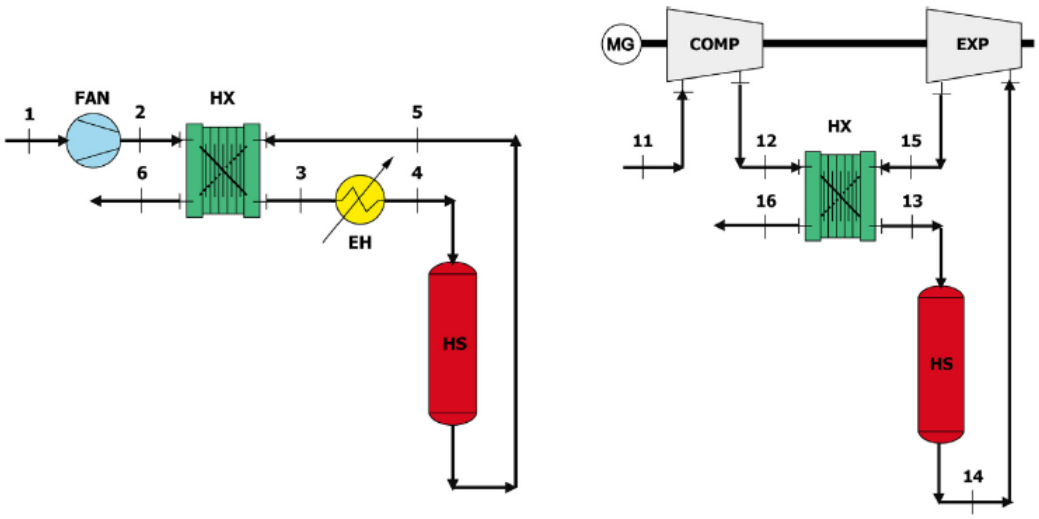

(a) *Charging phase* (b) *Discharging phase*

Figure 2.8: Schemes of the proposed plant [23].

In the discharge process, the air enters the compressor, then passes through the heat exchanger. Then, is heated up in the storage tank and, after that, it enters the compressor where is expanded. In the end it proceeds through the heat exchanger and is discharged in the external ambient (figure 2.8b).

Compared with other similar plant configurations (for instance [22]), here there is no need of a cold tank, and this reduces both the complexity and the costs of the system. Moreover, in this new plant arrangement, there is the need of install just two machines (COMP and EXP), while in other studies (such as [14]), four machines

were adopted, since they were required bot during the charging and the delivering phase.

The tank's arrangement (figure 2.9) is vertical, in order to prevent and avoid buoyancy-driven instabilities of the thermal front. The vessel is cylindrical and composed by an upper plenum, a packed bed and a lower plenum. During the charging phase the air enters from the top while during the delivery it flows from the bottom to the top. The elements used in the storage material are spheres of aluminum oxide. The most important aspect for the choice of the storage material is to adopt cheap, non-flammable and non-toxic materials. Moreover, the materials must be characterized by good thermal properties like the thermal diffusivity and conductivity.

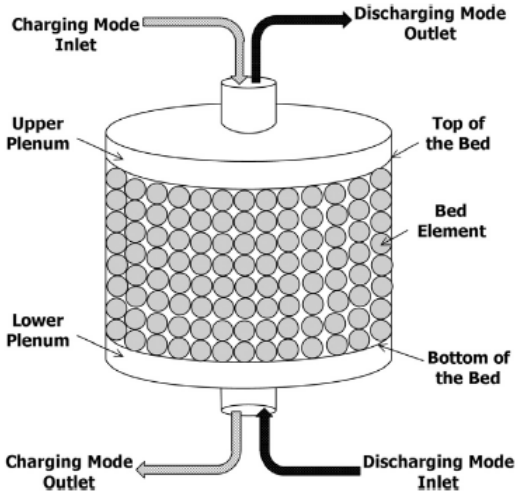

Figure 2.9: Tank's configuration, as proposed in [21].

2.3 The models of the storage tanks

In order to properly describe and predict the behaviour of the packed bed and the storage tank, several mathematical models have been proposed and analysed in the literature. To better familiarize with the one introduced by Benato et al. in [24], that is also the model adopted in this work, it is important to investigate and properly understand the various models previously proposed. According to the authors, three main models have been used in literature and all of them can describe accurately the time-varying behaviour of the storage device. In the following, these three models are analysed in order to evaluate the most important aspects of each of them and to properly understand how the model used in this work has been built.

2.3.1 Model 1: Howell et al.

The model was presented in 1982 by Howell et al [25]. The packed bed is schematized through different layers (in number equal to N) over the height of the tank L. Inside any layer, the temperature and the pressure are assumed uniform and constant through the bed element. According to this model the pressure drops can be written as:

$$\Delta p = C_f \cdot \frac{L \cdot G^2}{d \cdot \rho_f} \tag{2.1}$$

The parameter C_f is the so-called friction coefficient and G is the specific mass flow rate obtained as the ratio between the mass flow rate $\dot{m}$ and the cross sectional area of the tank A. d represents the equivalent diameter of the particle and ρ_f the density of the working fluid.

The temperature of the fluid along the bed can be calculated through the following relationship:

$$T^t_{f,i} = T^t_{s,i} + (T^t_{f,i-1} - T^t_{s,i})^{-\Phi_1} \tag{2.2}$$

The bed's temperature is obtainable as:

$$T_{s,i}^{t+\Delta T} = T_{s,i}^{t} + [\Phi_2 \cdot (T_{f,i-1}^{t} - T_{f,i}^{t}) - \Phi_3 (T_{s,i}^{t} - T_{amb})] \cdot \Delta t \tag{2.3}$$

The parameter Φ_1, Φ_2 and Φ_3 are defined respectively as:

$$\Phi_1 = \frac{h_v \cdot A \cdot L}{N \cdot (\dot{m} \cdot c_{p,f})} = \frac{NTU}{N} \tag{2.4}$$

$$\Phi_2 = N \cdot \frac{\dot{m} \cdot c_{p,f}}{\rho_s \cdot A \cdot L \cdot c_{p,s} \cdot (1 - \varepsilon)} \tag{2.5}$$

$$\Phi_3 = \frac{U_i \cdot \Delta A_i}{\dot{m} \cdot c_{p,f} \cdot \Phi_2} \tag{2.6}$$

In the previous expressions, Tf, i is the temperature of the i-th fluid layer; Ts, i is the temperature of the i-th layer of the packed bed. The density of the material of the packed bed is denoted as ρ_s, the specific heat at constant pressure of the solid material is $c_{p,s}$ and ε is the void fraction of the packed bed. $c_{p,f}$ is the specific heat of the fluid at constant pressure. The time step Δt is calculated as $\Delta T = (\rho_f \cdot L \cdot A \cdot \varepsilon)/(N \cdot \dot{m})$. NTU is the number of transfer units, U_i is the overall heat loss coefficient and ΔA_i represents the external area of a layer. h_v is the volumetric heat transfer coefficient and depends on the thermal conductivity of the fluid k_f, the hydraulic diameter d and the Nusselt number Nu according to the following expressions:

$$h_v = \frac{Nu \cdot k_f}{d^2} \tag{2.7}$$

To calculate these parameters it is possible to adopt the correlations proposed by Singh et al. in [26] and here reported:

$$Nu = 0.437 \cdot Re^{0.75} \cdot \Psi^{3.35} \cdot \varepsilon^{-1.62} \cdot \exp[29.03 \cdot (\log \Psi)^2] \tag{2.8}$$

Where:

$$Re = \frac{G \cdot d}{\mu_f} \tag{2.9}$$

The parameter μ_f is the dynamic fluid viscosity and $\Psi = \frac{A_s}{A_e}$ is the particle sphericity, defined as the ratio of the surface area of a particle of the same volume and the particle surface area.

In the end, the coefficient C_f is obtainable as:

$$C_f = 4.466 \cdot Re^{-0.2} \cdot \Psi^{0.696} \cdot \varepsilon^{-2.945} \cdot \exp[11.85 \cdot (\log \Psi)^2] \tag{2.10}$$

The model proposed by Howell et al. in [25] gives considerable success in the literature due to its simplicity. However, this fact is limiting in more complex applications or whenever time-accurate details are required, as highlighted in [24].

2.3.2 Model 2: McTigue et al. and White et al.

The second model analysed is the one proposed by McTigue et al. in [22]. According to the authors, the model is based on a quasi-steady analysis; the equations governing the heat transfer in the reservoirs are integrated in time in order to study and account for the thermal fronts. This is done since the energy and the exergy losses in the storage tanks depend on the time-history of their operation. As highlighted in the work [22], the main source of losses in the reservoirs are related to the frictional losses and the heat transfer irreversibilities. Since the heat leakages, with a proper level of insulation, are very low, they are not accounted in the model. The thermal losses are associated to a finite temperature difference between the gaseous working fluid and the storage material. To quantify these losses, the authors considered the model proposed by Schumann for packed beds [27]. The model assumes that the heat transfer is limited by surface effects (so, the internal thermal resistance of the particles can be neglected) and the flow is one-dimensional. Consequently, the energy equations for the gas and the solid can be expressed as:

$$\frac{\partial T_f}{\partial x} = \frac{T_s - T_f}{\ell} \tag{2.11}$$

$$\frac{\partial T_s}{\partial t} = \frac{T_f - T_s}{\tau} \tag{2.12}$$

The parameters T_f and T_s are the fluid and the solid temperatures respectively. ℓ is the lengths scale and τ is the time scale, defined as:

$$\ell = \frac{1}{St \cdot (1-\varepsilon) \cdot S_v} \tag{2.13}$$

$$\tau = \frac{\rho_s \cdot c_{p,s}}{St \cdot c_{p,f} \cdot G \cdot \rho_f} \tag{2.14}$$

St is the Stanton number $St = h/(G \cdot c_{p,f})$, G the mass flow rate of the gas per unit of area and S_v is the surface to volume ratio of the solid particle (in case of spherical particles is equal to $6/d$ where d is the particle diameter). The equations are obtained assuming steady flow through an infinitesimal layer of the packed bed (i.e., neglecting the unsteady gas energy and mass accumulation terms) and by computing the gas-to-solid heat transfer as the product of the local heat transfer coefficient, the interfacial area and the gas–solid temperature difference [22]. A number of refinements to this model are included to account for: unsteady accumulation terms for the gas; temperature dependence of the solid heat capacity; variations in density, viscosity and other gas properties. Most of these have only a minor impact, but the variation of cs can significantly affect the shape of the thermal fronts and hence the losses.

Starting on the model proposed, White et al. [28] developed modified version of Schumann's model introducing variable properties for the solid and the fluid, including momentum and mass continuity equations. Thus, it is necessary to consider the equations governing the heat and mass exchanges that occur in an infinitesimal control volume of the tank. The relationship for the heat exchange can be written as:

$$\delta\dot{Q} = A \cdot \delta x \cdot (1-\varepsilon) \cdot S_v \cdot h \cdot (T_f - T_s) \tag{2.15}$$

In this equation, the parameter h is the superficial heat transfer coefficient.

At this point, the equations governing the mass continuity, the momentum and the energy (both fluid and solid) in differential formulation can be written as:

$$\varepsilon \cdot \frac{\partial \rho_f}{\partial t} + \frac{\partial G}{\partial x} = 0 \tag{2.16}$$

$$\frac{\partial G}{\partial x} + \frac{\partial}{\partial x}\left(\frac{G^2}{\rho_f} + \varepsilon^2 \cdot (p - \rho_f \cdot g \cdot x)\right) = -\varepsilon(1-\varepsilon) \cdot \tau' \cdot S_v \tag{2.17}$$

$$\varepsilon \cdot \frac{\partial}{\partial t}(\rho_f \cdot e_f) + \frac{\partial}{\partial x}(G \cdot h_f) = (1-\varepsilon) \cdot S_v \cdot h \cdot (T_s - T_f) \tag{2.18}$$

$$\rho_s \cdot c_{p,s} \cdot \frac{\partial T_s}{\partial t} = S_v \cdot h \cdot (T_f - T_s) \tag{2.19}$$

The parameter τ' is the surface shear stress, p the pressure, g the gravity acceleration, x the axial coordinate, e_f is the internal energy per unit of mass of the fluid and h_f is represents the enthalpy of the fluid per unit of mass. As suggested in [28], to reduce the computational effort deriving from the resolution of the previous equations, the model can be simplified considering the model proposed by Schumann. To account for the contributions of time-dependant parameters, it is necessary to introduce a correction factor F, that can be defined as:

$$F = \frac{\varepsilon}{G \cdot c_{p,f}} \cdot \left(\frac{\partial p}{\partial t} - \rho_f \cdot c_{p.f} \cdot \frac{\partial T_f}{\partial t}\right) \tag{2.20}$$

This expression can be averaged and added to the fluid energy equation. Integrating the Schumann model accounting for the F factor, a semi-analytical model is obtained.

$$T_{f,i}^{t+\Delta t} = \left(\overline{T_s} + \overline{F} \cdot \ell\right) \cdot \left[1 - \exp\left(\frac{-\Delta x}{\ell}\right)\right] + T_{f,i-1}^{t+\Delta t} \cdot \exp\left(\frac{-\Delta x}{\ell}\right) \tag{2.21}$$

$$T_{s,i}^{t+\Delta t} = \overline{T_f} \cdot \left[1 - \exp\left(\frac{-\Delta t}{\tau}\right)\right] + T_{s,i-1}^{t} \cdot \exp\left(\frac{-\Delta t}{\tau}\right) \tag{2.22}$$

In the previous expressions the parameters $\overline{T_f}$ and $\overline{T_s}$ are the mean temperature of the fluid and the solid, defined respectively as:

$$\overline{T_f} = \frac{T_{f,i}^{t} + T_{f,i}^{t+\Delta t}}{2} \tag{2.23}$$

$$\overline{T_s} = \frac{T_{s,i-1}^{t+\Delta t} + T_{s,i}^{t+\Delta t}}{2} \tag{2.24}$$

The equation governing the mass continuity (2.16) can be implemented as:

$$G_i^{t+\Delta t} = G_{i-1}^{t+\Delta t} + \varepsilon \cdot \frac{\Delta x}{\Delta t} \cdot \left(\rho_{f,i}^{t} - \rho_{f,i}^{t+\Delta t}\right) \tag{2.25}$$

2.3.3 Model 3: Desrues et al.

The third model analysed is the one proposed by Desrues et al. in [14]. As highlighted by the authors, the transient phenomena play a central and critical role in the system behaviour. The pressure does not remain constant during a cycle and the thermal fronts changes, due to the convective heat exchanges and the thermal diffusivity of the materials employed. Accdording to this, the authors proposed a one-dimensional finite volume method for the discretization of the tank. The equations that are used to describe the tank are here presented:

$$\frac{\partial \rho_f}{\partial t} + \frac{\partial (\rho_f \cdot v_f)}{\partial x} = 0 \tag{2.26}$$

$$\frac{\partial (\rho_f \cdot T_f)}{\partial t} + \frac{\partial (\rho_f \cdot T_f \cdot v_f)}{\partial x} = \frac{4 \cdot Nu \cdot k_f}{c_{p,f} \cdot (d_h)^2} \cdot (T_s - T_f) \tag{2.27}$$

$$\rho_s \cdot c_{p,s} \cdot \frac{\partial T_s}{\partial t} + k_s \cdot \frac{\partial^2 T_s}{\partial x^2} = \frac{\varepsilon}{1-\varepsilon} \cdot \frac{4 \cdot Nu \cdot k_f}{(d_h)^2} \cdot (T_f - T_s) \tag{2.28}$$

In particular, the equation 2.26 is the mass conservation while the equations 2.27 and 2.28 are the energy conservation inside the gas and the solid respectively.

In the model, the pressure drops are accounted through the equation 2.29 and the ideal gas equation of state 2.30, reported in the following:

$$\frac{\partial p}{\partial x} = -C_f \cdot \frac{4}{d_h} \cdot \frac{1}{2} \cdot \rho_f \cdot v_f^2 \tag{2.29}$$

$$p = \rho_f \cdot r \cdot T_f \tag{2.30}$$

The proper evaluation of the heat transfer and pressure drops coefficients requires the Nusselt number and the friction factor correlations. In our case, the adopted correlations concerning the spheres packing geometry are reported in the following expressions. In particular, the hydraulic diameter is defined as:

$$d_h = \frac{\varepsilon}{1-\varepsilon} \cdot Re \tag{2.31}$$

The hydraulic Reynolds number, related to the superficial one, can be written as:

$$Re_h = \frac{1}{1-\varepsilon} \cdot Re \tag{2.32}$$

Re_h is used to determine the friction factor, according to the following expressions:

$$C_f = 2 \cdot \left(\frac{A}{Re_h} + B \right) \tag{2.33}$$

In 2.33, that represents the Ergun equation [29], we have $A = 150$ and $B = 1.75$. The correlation for the Nusselt number is given by Wakao et al. in [30] and is reported in the following expression:

$$Nu = 2 + 1.1 \cdot Pr^{1/3} \cdot Re^{3/5} \tag{2.34}$$

The Prandtl and the Reynolds numbers are respectively defined as:

$$Pr = \frac{\mu_f \cdot c_{p,f}}{k_f} \tag{2.35}$$

$$Re = \frac{G \cdot d}{\mu_f} \tag{2.36}$$

2.3.4 Model 4: Benato et al.

The model proposed by Benato et al. in [24] (TES-PD) relies on the formulation proposed by Desrues et al. in [14]. Starting from this model, the authors improved it integrating a set of parameters that affect the behaviour of the storage tank, such as the space and time variability of all the thermophysical properties of the fluids and the materials employed in the system, the overall heat loss coefficient and the solid effective thermal conductivity of the material. According to the authors the model of Desrues et al. ([14]) is the most advanced model available in literature to describe the behaviour of the storage tank. Anyway, it assumes constant solid and fluid properties, that is a strong limitation that leads to uncertainties and the impossibility to adopt the model for the most advanced storage materials. Thus, if properly modified, the model of Desrues et al. can be suitable for the updating of all the thermophysical properties in both space and time. In particular in [24], the authors introduce these properties following a procedure similar to the one described by McTigue et al. in [22]. Differently from this model, the authors decided to acquire the material properties from the National Institute of Standards and Technology database (NIST - https://janaf.nist.gov/), while the fluid properties were taken from the CoolProp library. Following this procedure, the properties and their variability were properly considerd, updating their values considering the actual temperature.

Regarding the heat loss coefficient, it is accounted by only the model proposed by Howell et al. in [25], but it is a parameter of central importance for the exact description of the behaviour of the tank. Introducing this hypotheses the model can be written as:

$$\frac{\partial \rho_f}{\partial t} + \frac{\partial (\rho_f \cdot v_f)}{\partial x} = 0 \tag{2.37}$$

$$\frac{\partial (\rho_f \cdot T_f)}{\partial t} + \frac{\partial (\rho_f \cdot T_f \cdot v_f)}{\partial x} = \frac{1}{\varepsilon} \cdot \alpha \cdot (T_s - T_f) \tag{2.38}$$

$$\frac{\partial (\rho_s \cdot c_{p,s} \cdot T_s)}{\partial t} + \frac{\partial}{\partial x}\left(k_{s,eff} \cdot \frac{\partial T_s}{\partial x}\right) = \frac{c_{p,f}}{1-\varepsilon} \cdot \alpha \cdot (T_f - T_s) - U_i \cdot \frac{C_u}{1-\varepsilon} \cdot (T_s - T_{amb}) \tag{2.39}$$

In particular the equation 2.37 represents the conservation of the mass, 2.38 is the fluid energy conservation and 2.39 is the solid energy conservation.

It is necessary to include the pressure drops and the ideal gas equation of state:

$$\frac{\partial p}{\partial x} = -C_f \cdot \beta \cdot \frac{1}{2} \cdot \rho_f \cdot v_f^2 \tag{2.40}$$

$$p = \rho_f \cdot r \cdot T_f \tag{2.41}$$

In the previous expressions t is the time and x is the axial tank coordinate, L is the tank's length. ρ_f, v_f, T_f and p are the fluid density, velocity, temperature and pressure. The temperature and the density of the storage material are T_s and ρ_s, respectively. k_f and $k_{s,eff}$ are the fluid and the solid effective thermal conductivity; $c_{p,f}$ and $c_{p,s}$ are the fluid and the solid specific heat coefficients at constant pressure. ε is the void fraction, T_{amb} is the ambient temperature and r is the specific constant of the gas. The two parameters α and β derives from the model described in [14] and are typical for the material geometry adopted in the model. In particular, for spheres packing α and β are equal to:

$$\alpha = \frac{6 \cdot Nu \cdot k_f}{c_{p,f} \cdot d^2} \tag{2.42}$$

$$\beta = \frac{1-\varepsilon}{d \cdot \varepsilon} \tag{2.43}$$

In the previous expressions the parameter d denotes the particle diameter. U_i represents the overall heat loss coefficient and $C_u \cdot (1-\varepsilon)^{-1}$ is the external surface to volume ratio. In particular, for spheres packing geometry, the parameter C_u is defined as:

$$C_u = \frac{2 \cdot \pi}{A} \cdot \sqrt{\frac{A}{\pi}} \tag{2.44}$$

The calculation of Nusselt number and the friction coefficient are performed following what reported in [14].

As highlighted in [24], by comparing the model proposed by Benato et al., with the one proposed by Desrues et al. in [14], it can be observed that the equation regarding the mass conservation 2.37 and the one related to the conservation of the fluid energy 2.38 remain unaltered. Instead, the equation 2.39, associated to the conservation of the solid energy, accounts now for the time-variability of the thermophysical parameters and for the heat losses through the external surface. These improvements are of crucial importance for the proper analysis of the behaviour of the system under analysis.

This model is the one adopted in the work here presented. It is implemented in MatLab environment through the creation of a function, that is able to describe the behaviour of the thermal energy storage tank. The function allows the calculation of temperature and pressure at the outlet of the storage tank, given the conditions of the operative fluid at the inlet of the device. The function is used to describe the behaviour of the overall system, as described in [23].

2.4 The concept of Virtual Power Plant

A Virtual Power Plant (VPP) is a new and innovative concept in the energy system field. The VPP can be defined as a "cloud-based platform that aggregates distributed energy sources, loads of various nature, storages and electric vehicles, providing real-time monitoring via a bidirectional communication system, aims to establish a distributed and decentralized power plant enhancing energy management and trading across the power system" [31]. In other words, the VPP consists of an aggregation of distributed generators, storage systems, controllable loads, metering, communication and other technologies [32], and allows the improvement of the energy management efficiency and facilitate the energy exchanges and tradings. As highlighted in the work of Benato et al. [3], a VPP is an aggregator that connects generators, load and energy storages as a single entity of the electrical grid. Depending on the goals of the players involved in the system, the Virtual Power Plant can assume a central role. As highlighted in various studies (as reference, [33, 34]), the construction of centralized renewable energy sources power plants requires significant capital investment while transmission loss and other costs still exist. A comprehensive management solution is required to solve challenges such as the high risk of market participation, unilateral pricing and energy trading complexity [31].

As reference, we can consider the work of Benato et al. [3], in which the system composed by photovoltaic plant and energy storages is connected to the electrical grid and is treated as a Virtual Power Plant. The scope of the VPP under analysis was to prevent the peak in the power production, typical of a photovoltaic plant: it is well known that during the peak hours the production of the PV plant is very high, while in the night it is null. Discontinuities in the power production can cause instabilities that must be reduced or avoided to preserve the quality of the distribution and transmission of the electricity along the grid. To proceed in this way, the authors suggested to send part of the energy generated by the photovoltaic plant during the central hours directly to the electrical grid, while the remaining part

is used to charge the storage system. In the period in which the production is null, the energy stored in the tank in form of sensible heat, is used to generate electricity to be provided to the electrical grid. During this phase, the power produced is maintained constant.

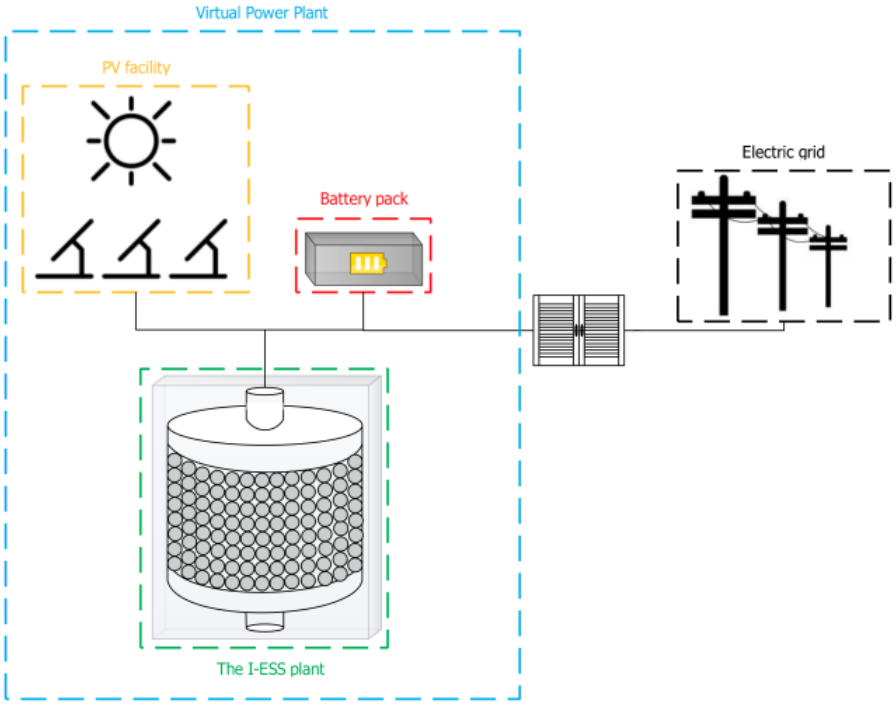

Figure 2.10: Schematic representation of the VPP, as depicted in [3].

As we can see in the Figure 2.10 reported above, the system includes a battery park too. This device is required to store the energy when the power provided by the PV plant is less than a predefined power and is also not sufficient to charge the storage tank. The energy that is accumulated in the battery park is used to start the system when the discharging phase take place.

We have seen that the authors worked to reduce the fluctuation in the grid, observing the power values at the corresponding interconnection node between the plant and the grid. Once the value of the power has been chosen, the virtual power

plant is optimized in order to provide that power for the greatest number of hours per day. The photovoltaic production is reconstructed considering quarters of hour, in order to evaluate the number of hours in which the previously explained scope is reached. Starting from the grid needs, the available space in the photovoltaic facility and that the size of the thermal storage tank must correspond to the energy that need to be stored at the required temperature, the tank, the compressor and the turbine are designed. The size of the packed bed comprising the thermal energy storage, must be adjusted such that the bed absorbs the greatest amount of energy made available by the heat transfer fluid passing through the bed during the charging phase. It is important to highlight that there is not a precise criterion for designing the packed bed and for the choice of the machines of the plant such as the gas turbine and the fan machines [3].

The authors investigated also how the starting month of operation affects the behaviour of the overall performances of the plant. From this kind of study, the authors find out that the energy recovered was a little bit higher when the plant starts its operation in January. Anyway, this variations becomes negligible during the second year of operation of the plant.

Proceeding with the study of the temperature distribution inside the storage tank, it was highlighted that during the summer season the tank is almost fully charged, whereas in winter the temperature of some sections of the tank becomes lower than the air temperature after the compression phase: when the amount of energy to be stored is low, some tank sections are not active and the heat transfer to the external environment becomes more critical. As result, during the cold months, in which the irradiance is lower, the photovoltaic system may recharge partially the thermal energy storage in a not so efficient way. This aspect strongly depend on the choice of the management strategy of the system [3].

The article of Rouzbahani et al. [31] provides a comprehensive review of VPP applications for energy management in power grids. The authors tried to highlight the most common scheduling techniques in energy management using VPP. Gen-

erally, the main objectives in the scheduling program are the minimization of the costs related to the generation, transmission, distribution, and maintenance, the reduction of the bills (important in particular for the users); moreover, the minimization of the greenhouse gas emissions and the maximization of the performances of the power system are other central objectives that can be reached through the implementation of a Virtual Power Plant. In the optimization process, it is necessary to consider both economical and technical aspects. One of the most critical aspects is dealing with uncertainty and forecasting of renewable energy sources, and it requires to reach an optimal scheduling procedure of the VPP. In literature, several different scheduling methods have been proposed, and the authors have tried to collect the most significant ones. In general terms, the optimum scheduling of VPP is a multi-objective problem aiming to maximize the profit while minimizing the cost and loss. Operation scheduling aims to minimize the expenses and maximize the profits and the revenue for customers, consumers, and providers considering, at the same time, the environmental impact. On the other hand, the main technical objective is the achievement of the optimal system's performances, such as the stability, the reliability, the security, and the quality of the transmission. The authors individuate three different categories to formulate the optimal operation scheduling of the virtual power plant. We can consider the "classic methods", based on linear programming: it is possible to apply these methods whenever the aspects we want to maximize or minimize are described (in a simplified way) by linear functions. The "heuristic and metaheuristic methods" aim to achieve a specific result for a problem that is tested by considerable experiments, making a sort of trade-off between the accuracy and the computational effort. Lastly, there is the possibility to use the "learning-base methods" exploiting artificial intelligence and machine learning. The authors [31] observed that not only the technical constraints of the network have a substantial impact on the scheduling algorithm, but also the economic aspects are important. Therefore, it is clear that a comprehensive and intelligent scheduling algorithm requires both technical and economical constraints. There is also the

need to account for the uncertainty behavior of the energy sector market, which is strongly dependent on the floating of socioeconomic aspects.

Seen the great importance of the concept of the Virtual Power Plant, and following what reported in the work of Benato et al. [3], we are going to consider the system described in this work as a VPP.

Chapter 3

Model of the system

To properly understand and study the behaviour of the storage system, it is necessary to build a model able to describe the functioning of the storage device and of the various other components that constitute the system. In particular, we are going to consider the system as described by Benato et al. in [23] and [3]. In particular, for the charging phase, the corresponding system comprehends a fan, a heat exchanger, an electric heater and the storage tank as we can see in Figure 3.1.

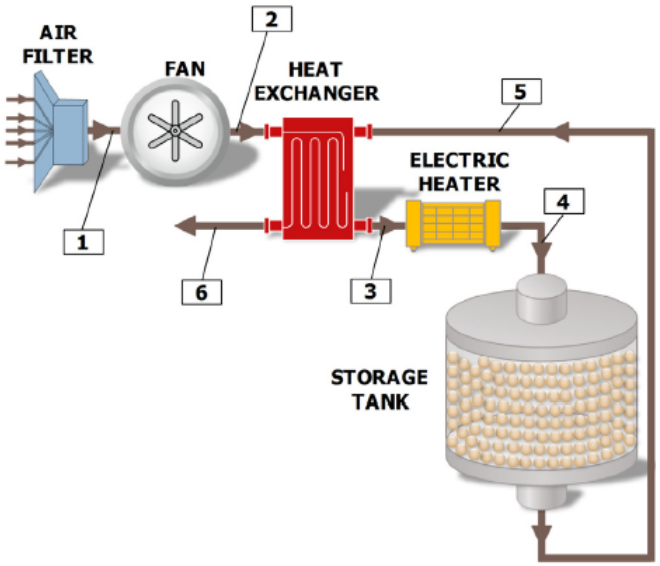

Figure 3.1: Scheme of the system for the charging phase as reported in [23].

Similarly, for the discharging phase we have a compressor, the heat exchanger, the storage tank and a turbine. The turbine is coupled to an electric generator able to produce electrical energy (Figure 3.2).

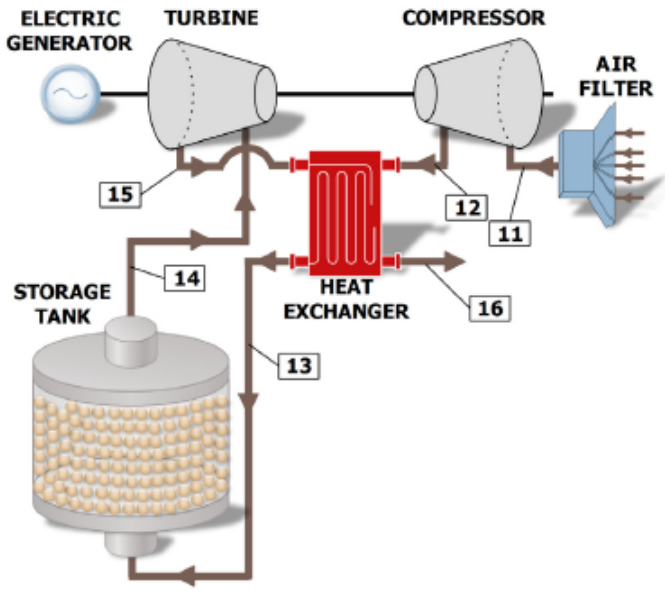

Figure 3.2: Scheme of the system for the discharging phase as reported in [23].

The working fluid used in the system is the ambient air and the storage medium is aluminum oxide.

To describe the behaviour of the storage device, the parameters used in the MatLab algorithm of the model of Benato et al, are reported in the following:

- The inlet conditions of pressure, temperature and mass flow rate, respectively designed as, T_{in}, p_{in} and $\dot{m}_{in}$. The inlet conditions are related to the behaviour of the other devices present in the system. In particular, the inlet temperature, during the charging phase, depends on the electric heater. In the simulations performed the inlet temperature is maintained constant and is assumed equal

to 1000 °C. This choice is connected to the maximum temperature feasible with the material used in the storage tank. During the discharging phase, the inlet temperature is connected to the behaviour of the heat exchanger, and is determined through an algorithm implemented in MatLab environment. The inlet pressure depends on the compression devices used in the system (fan during the charge and compressor during the discharge). The mass flow rate changes in the various simulations, considering different management strategies of the IT-ESS.

- Height L, volume V and number of layers of the tank N. The number of layers of the tank describes the degree of detail of our calculations, and is the number of subdivisions of the tank of thickness equal to $\Delta L = L/N$. For each subdivision the algorithm proceeds with the balances of mass and energy. In our simulations, the number of layers assumed is equal to 60, that can be considered a good compromise between quality of the results and speed of the algorithm used in the description of the system. The choice of the volume and of the height of the tank is related to the different management strategies of the system and on the limit related to the Nu number, ad described in [26].

- Ambient temperature T_{amb} and pressure p_{amb}.

- Maximum temperature T_{max}.

- Density of the storage material ρ_s and its thermal conductivity K_s (this last parameter is assumed equal to 0 $\mathrm{W/(m \cdot K)}$ [24]).

- Specific heat $c_{p,s}$ of the storage material. The values of this parameters are derived from the NIST database.

- Thermal transmittance of the storage tank U.

- Equivalent diameter of the storage particle d and their sphericity Ψ (that is assumed equal to 1).

- Void fraction of the tank ε. Again, the choice of this parameter is related to the limit imposed in [26].
- Specific heat, density, thermal conductivity, molar mass and dynamic viscosity of the working fluid (air in our case). These data are derived from the RefProp database.
- Diameter of inlet and outlet ducts of the storage tank D.

The values of the parameter used are reported in the following Table 3.1.

$\boldsymbol{T_{amb}}$ **[°C]**	15 - 25
$\boldsymbol{p_{amb}}$ **[kPa]**	101.325
$\boldsymbol{T_{max}}$ **[°C]**	1000
$\boldsymbol{\rho_s}$ **[kg/m^3]**	3990
$\boldsymbol{U}$ **[W/(m^2 · K)]**	0.7
$\boldsymbol{d}$ **[m]**	$50 \cdot 10^{-3}$
$\boldsymbol{\varepsilon}$ **[−]**	0.4
$\boldsymbol{D}$ **[m]**	1

Table 3.1: Parameters adopted in the simulations

To describe the other devices used, some other parameters are introduced. For the turbomachines (Table 3.2) it is important to introduce the politropic efficiency η_{pol} and the electric efficiency of the motors η_{el}. Moreover the compression ratio is particularly important for the fan and the compressor. The heat exchanger is characterized by a certain efficiency ε. For the electric heater a conversion efficiency between electrical and thermal energy is introduced η_{el} (Table 3.3).

	η_{pol} [−]	η_{el} [−]
Fan	0.85	0.95
Compressor	0.85	0.95
Turbine	0.85	0.95

Table 3.2: Parameters of the turbomachines.

Electric heater	η_{el} [−]	0.95
Heat exchanger	ε [−]	0.8

Table 3.3: The electric efficiency and the heat exchanger one, adopted in this work.

It is necessary to define a limit to consider the charging and the discharging processes completed. In particular, for the charge, it is assumed to consider the temperature of the working fluid at the outlet of the storage tank higher than 950 °C. This parameter is of fundamental important, since it strongly affects the duration of the charging process: in fact, the closer it is to the maximum temperature of the system, the longer will be the duration of the charge. Typical values that can be adopted are between 50 to 150 K lower than the maximum temperature of the cycle. For the discharging phase, the limit will be again the temperature reached by the air at the outlet of the storage tank. In particular, in our simulations, this limit will be equal to a temperature of 1010 K. This strategies for the limits in the charging/discharging processes is valid when we want to perform a complete charge/discharge: in some simulations performed, the limits are related to the availability of power during a day. For example, the discharge typically occurs during the hours in which there is not availability of power to be used to charge the storage systems, and this occurs during the night. In these cases, the charge occupies the central hours of the day, in which the power allows the storing of energy. Anyway, for sake of clarity, these limits will be specified for each simulation performed, in order to properly understand which is the scenario we are going to reply and to

properly identify the context of the simulation.

Another parameter of central importance is the aspect ratio, that is used to properly evaluate the dimensions of the storage tank starting from its volume. This parameter can be defined as the ratio between the height of the tank L_{tank} and its diameter d_{tank}, in case of a cylindrical-shaped tank.

$$AR = \frac{L_{tank}}{d_{tank}} \tag{3.1}$$

To properly understand the effect and the importance of this parameter, it was decided to perform some simulations. In this way, we can study how the aspect ratio affects the duration of a charging/discharging phase and the pressure drops inside the storage material. For this preliminary simulations, the values adopted for the mass flow rate, the volume of the storage tank and the pressure ratios of the fan and the compressor are reported in the following Table 3.4 and Table 3.5. This values are chosen considering a typical volume of storage devices. The mass flow rates are related to typical sizes of the turbomachines adopted, such as the corresponding pressure ratios.

Charge		
$\boldsymbol{V}$	$\boldsymbol{\dot{m}}$	$\boldsymbol{r_{c,fan}}$
$[\mathbf{m^3}]$	$[\mathbf{kg/s}]$	$[-]$
75	3.4	1.4

Table 3.4: Mass flow rate, volume and pressure ratio used during the charging phase.

When several simulations were completed, we collected the data to obtain the trend of the duration of a complete charge/discharge phases and the pressure drops as a function of the aspect ratio.

Charge		
V	$\dot{m}$	$r_{c,comp}$
$[m^3]$	$[kg/s]$	$[-]$
75	3.4	1.4

Table 3.5: Mass flow rate, volume and pressure ratio used during the discharge.

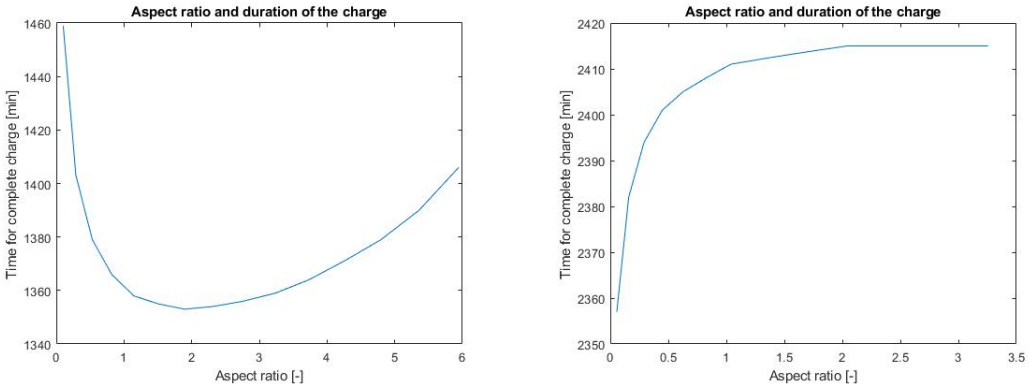

(a) *Charging phase* (b) *Discharging phase*

Figure 3.3: Duration of the charge and the discharge as a function of the aspect ratio.

In the Figure 3.3, we can observe that a too high aspect ratio have an impact on the time to perform a complete charging and discharging process. Anyway, as we can see from the figure, the duration of the two processes does not change significantly: the differences between the worst and the best case are lower than 1 hour.

In the following Figure 3.4, we can see that the choice of the aspect ratio is really important. A too high value leads to very high pressure losses. Thus, the proper choice of this parameter results extremely important.

At this point, we have to consider another aspect linked to the aspect ratio: the model adopted in the description of the behaviour of the thermal storage system

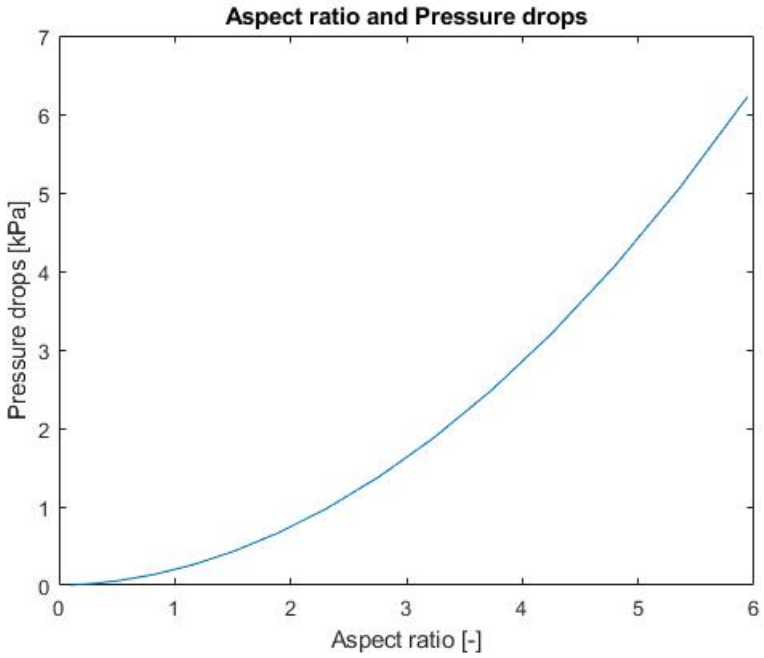

Figure 3.4: Pressure drops as a function of the aspect ratio.

considers the correlations proposed by Singh et al. in [26], for the calculation of the Nu number:

$$Nu = 0.437 \cdot Re^{0.75} \cdot \Psi^{3.35} \cdot \varepsilon^{-1.62} \cdot \exp[29.03 \cdot (\log \Psi)^2] \tag{3.2}$$

The correlation here reported, is valid within a specific range of the mass velocity G, defined as the ratio between the mass flow rate and the section of the storage device:

$$G = \frac{\dot{m}}{A} \tag{3.3}$$

The limits used in the work of Singh et al. are reported in the following Table 3.6: for sake of clarity, besides the limits of the mass velocity are reported also the limits for the sphericity of the particles and the void fraction. In our case, the sphericity and the void fractions are assumed the same for all the various simulations and are inside the limits valid for the correlation of Singh et al.

$\boldsymbol{G}$ $[\mathbf{kg/(s \cdot m^2)}]$	0.155 - 0.266
$\boldsymbol{\Psi}$ $[-]$	0.55 - 1
$\boldsymbol{\varepsilon}$ $[-]$	0.306 - 0.63

Table 3.6: Limits according to Singh et al. [26]

Focusing in particular on the mass velocity and its definition, we can understand that changing the value of mass flow rate and maintaining fixed the volume, we are changing the aspect ratio for which the correlation is valid. Thus the choice of the height of the storage tank is performed starting from the limits of the mass velocity. In fact, we have that:

$$L_{tank} = \frac{V}{A} \tag{3.4}$$

Where V and A are the volume and the area of the base of the tank respectively. Moreover, we have:

$$d_{tank} = 2 \cdot \sqrt{\frac{A}{\pi}} \tag{3.5}$$

Thus:

$$AR = \frac{V}{A} \cdot \frac{1}{2 \cdot \sqrt{\frac{A}{\pi}}} \tag{3.6}$$

At this point, knowing the value of G ($G_{max} = 0.266$ kg/(s $\cdot$ m^2) and $G_{min} = 0.155$ kg/(s $\cdot$ m^2)), and the mass flow rate $\dot{m}$, it is possible to individuate the range of aspect ratios for which the correlation proposed by Singh results valid. Moreover, it is possible to individuate the values of height of the storage tank, corresponding to the two values of the aspect ratio.

Chapter 4

Size of the storage system

It is well know that one of the most important aspects of the storage system regards the proper choice of the volume of the tank. In this chapter we want to investigate how it is possible to individuate which could be the proper volume according to different strategies. The choice of the volume depends on the energy we want to store and the energy that we can produce during the discharging phase. Moreover, it is important to understand how to use the storage tanks, when coupled with renewable energy sources, with the aim of the mitigation of the fluctuations in the production of these sources. In this way we can obtain a higher quality in the generation and the distribution of the electric energy, in scenarios in which the renewable energy penetration is assuming a more central role.

In our case, we are going to consider the energy produced by a photovoltaic field, located in Portoscuro, Sardinia, and we want to understand how to properly store it in our device. The PV plant is characterized by a peak power of 10.316 MW_p, the panels are oriented by 32° and the annual mean energy output is around 16 GWh. A production profile of the photovoltaic plant is created for a mean day for each month of the year. The reconstruction of these curves is done considering quarters of hours. As reference, in the following Figure (4.1), the trend of a day in January is presented. The shape of the curve is the typical profile of power produced in a photovoltaic plant: the curve presents a maximum in correspondence of the central

hours of the day, in which the solar radiation able to reach the panels is higher, while during the night the production is null.

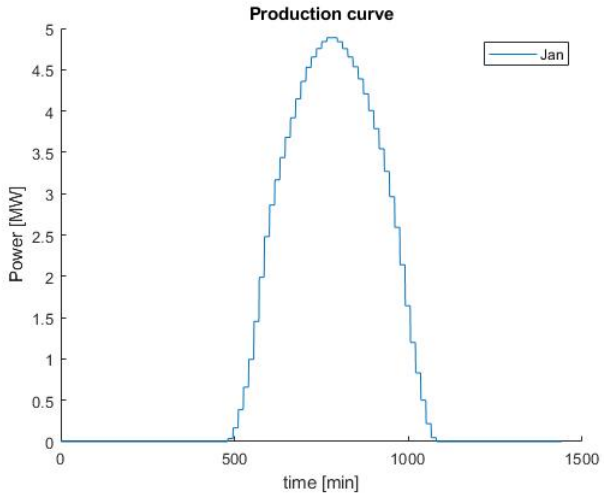

Figure 4.1: Profile for the power produced in a typical day of January.

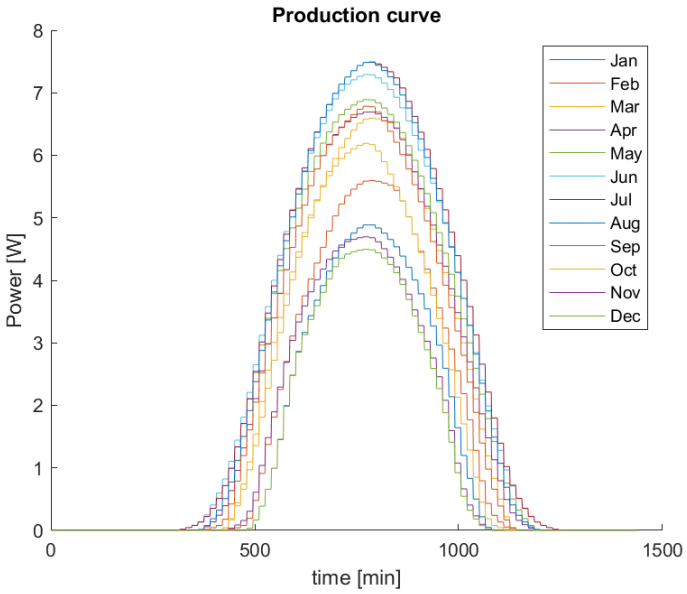

Figure 4.2: Profiles of the power produced in each month of the year.

Comparing the curves for each month of the year, we can observe that the months with the maximum and the minimum power produced are July and December, respectively.

4.1 Store all the energy produced in a day with the tank at ambient temperature

At this point, we have to understand which is the best strategy in the choice of the volume of the storage system, performing different kinds of analysis. First of all, we want to individuate the volume considering to store all the energy produced in a day by the photovoltaic plant. Thus, starting from the curves of the power produced along the day, and exploiting an environment like MatLab, it is possible to determine the electrical energy E_{el} performing the integral of the curves along the day. The charging of the storage device is performed through the usage of an electric heater, characterized by a certain efficiency η_{el}. At this point, knowing the energy to be accumulated, the mass of storage medium required can be evaluated as:

$$m_s = \frac{E_{th}}{c_{p,s} \cdot (T_{max} - T_{amb})} \tag{4.1}$$

In the equation 4.1, $c_{p,s}$ is the specific heat of the material, T_{max} is the maximum temperature achieved in the storage tank, T_{amb} refers to the temperature of the external environment and E_{th} is the thermal energy to be stored calculated as the product of the electrical energy produced by the photovoltaic plant and the electrical efficiency of the heating device used:

$$E_{th} = E_{el} \cdot \eta_{el} \tag{4.2}$$

In the present work we have seen that the storage tank is made of randomly packed spheres of solid materials like rocks, metals, concrete, and so on. A typical parameter that is used to describe the fraction of the storage device occupied by air is the void fraction ε. Once the mass is evaluated, considering the density of the storage material ρ_s and the void fraction, it is possible to calculate the volume of the device:

$$V_s = \frac{m_s}{\rho_s \cdot (1 - \varepsilon)} \tag{4.3}$$

The material adopted for the packed bed is alumina (aluminum oxide). In the following Table 4.1, the main characteristics of the storage material are reported, as well as the electric efficiency assumed for the heating device:

ε [−]	η_{el} [−]	T_s [°C]	ρ_s [kg/m^3]
0.4	0.95	1000	3990

Table 4.1: Parameters used in the calculation of the volumes of the storage tank.

Thus, the results obtained from the calculations previously explained are reported in the following Table 4.2:

	Jan	**Feb**	**Mar**	**Apr**	**May**	**Jun**
E_{el} [MJ]	104760	129960	165240	178920	191160	205200
V_s [m^3]	35.8	44.4	56.5	61.1	65.3	70.1
	Jul	**Aug**	**Sep**	**Oct**	**Nov**	**Dec**
E_{el} [MJ]	210240	202680	172080	146160	104400	93960
V_s [m^3]	71.8	69.3	58.8	49.9	35.7	32.1

Table 4.2: Electric energy and the corresponding volume for each month.

In particular, from Table 4.2, we can observe that the month characterized by the largest production, and thus by the largest volume, is July; instead, the month with the lowest production and volume results to be December.

In the following Figure 4.3 and Figure 4.4, the power production profiles of the months of July and December are reported. In the specific, we can clearly observe

that the power produced during the month of July reaches a higher value with respect to the month of December: in July the peak is around 7.5 MW, while in December the peak power reached during the day is around 4.5 MW. Moreover, we cal also see that there is a greater production in July with respect to December, and this is due to the different amount of energy that reaches the surface of the Earth in the two months.

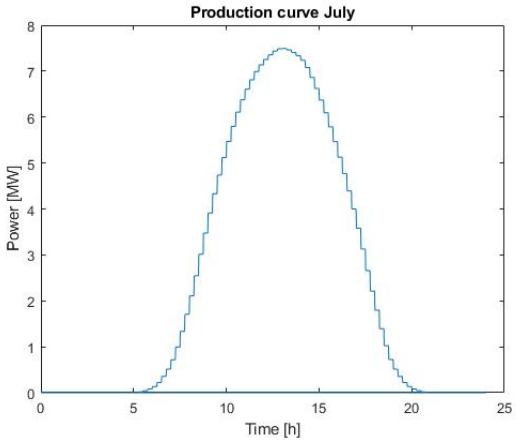

Figure 4.3: Profile for the power produced in a typical day of July.

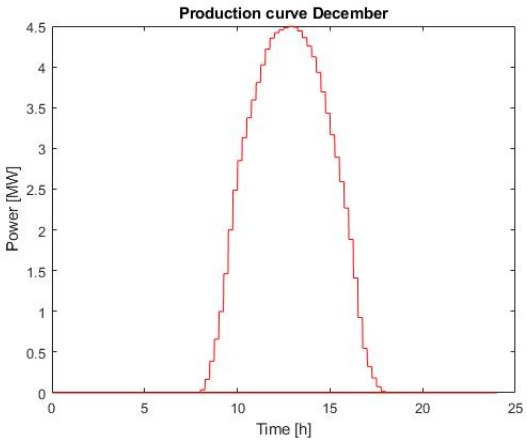

Figure 4.4: Profile for the power produced in a typical day of December.

4.2 Store all the energy produced following the power production curve of the PV plant

At this point, we have to consider that the storage device is part of a system and we have to account for the behaviour of the other components and, in particular, we have to consider the non constant power produced by the photovoltaic plant along the day. For this reason we are going to perform some simulations changing the mass flow rate to follow the production curve. The power produced by the photovoltaic plant is used to feed both the electric heater and the fan.

Analysing the results of some preliminary simulations performed without accounting for the limits imposed by Singh ([26]) for the month of July, we observed that the mass flow rate spaces from 0 to around 7 kg/s. A mass flow rate lower than 0.1 kg/s is not a valid value, since it results to be too low. Consequently, we decided to consider this as lower limit for the mass flow rate admissible during the charging process. In other words, the charging process starts when the mass flow rate is greater than 0.1 kg/s.

To account for the real behaviour of the plant coupled with the PV plant, it is necessary to perform a simulation able to reproduce the daily behaviour of the system, keeping in consideration both the charging and the discharging phases. Thus, this second simulations are structured considering to perform different charging/discharging cycles. The duration of the charging phase is determined from the PV production curves. In particular we assumed to perform the charge when the power produced by the plant is non null.

	July
Charge	960 min = 16 h
Discharge	480 min = 8 h

Table 4.3: Duration of the charge and the discharge for July.

	December
Charge	600 min = 10 h
Discharge	840 min = 14 h

Table 4.4: Duration of the charge and the discharge for December.

In the prevuous Table 4.3 and 4.4 we have reported the duration of the charging and the discharging processes.

At the end of the cycle of charging/discharging process, a last charging phase is performed, to determine the temperature of the air at the outlet of the storage system close to the end of the phase. If this temperature results too high (with respect to a certain target value, assume equal to 950 °C), the starting volume is increased. We proceed in this way until the volume able to store all the energy produced by the photovoltaic plant is obtained. We are interested in the evaluation of the maximum and minimum volumes: consequently, we are going to simulate the behaviour of the system considering just the months of July and December, characterized, as we have previously seen, by the highest and the lowest energy production respectively.

The starting value of the volume in both the situation was the value obtained with the previous simulations, in which we considered to store all the energy produced along the day. Thus, for the month of July we considered the volume equal to 71.8 m^3 and for December we started with a volume equal to 32.1 m^3.

According to this, we performed the simulations for the month of July and December. In these first simulations we were not accounting for the limits imposed by Singh [26]. Thus, all the mass flow rates have been considered acceptable (if greater than 0.1 kg/s). The characteristic parameters of these two simulations, and the results obtained are reported in the following Table 4.5.

July		
$\mathbf{V_{final}}$	$[\mathbf{m^3}]$	300
$\mathbf{L}$	$[\mathbf{m}]$	3
$\mathbf{r_{c,fan}}$	$[-]$	1.2
$\mathbf{\dot{m}_{discharge}}$	$[\mathbf{kg/s}]$	3.9
December		
$\mathbf{V_{final}}$	$[\mathbf{m^3}]$	46
$\mathbf{L}$	$[\mathbf{m}]$	3
$\mathbf{r_{c,fan}}$	$[-]$	1.2
$\mathbf{\dot{m}_{discharge}}$	$[\mathbf{kg/s}]$	3.9

Table 4.5: Results and parameters used in the first simulations performed.

We can see that the volumes calculated in these second simulations are greater with respect to the ones obtained in the first calculations. This is determined by the fact that now we are studying the real behaviour of the storage device, and we have to consider the duration of the charging and the discharging phases. In particular, we need to consider that after the first charge/discharge cycle, the storage device is characterized by a temperature that is different with respect to the ambient one. Consequently, using the volume used in the first analysis, it is not sufficient to store all the energy produced in the second day, and so on. Trough the simulations performed, we have considered a series of charging/discharging processes to verify if all the energy can be accumulated. In particular, we have performed 7 charges and 7 discharges, and at the end the temperature at the outlet of the storage tank is individuated. At the end of the simulations we have observed that the volumes to store all the energy, considering the constrains indicated in the previous passages, is equal to 300 m^3 for July and to 46 m^3 for December.

For sake of clarity, we decided to report also the values of the temperature in

the various point of the cycle, for the month of July. In the following Figure 4.5, we considered the trends of the various temperatures during the charging process.

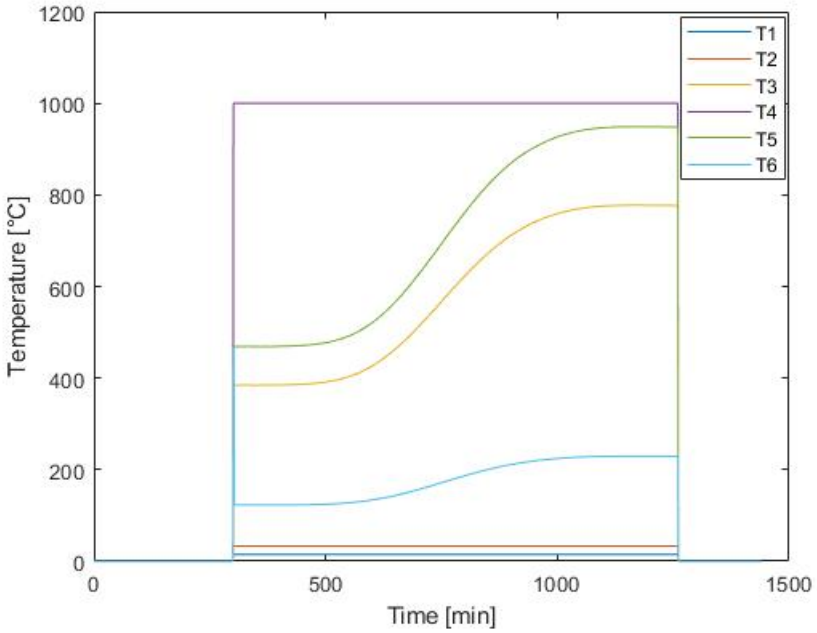

Figure 4.5: Temperature profile for July for the various points of the cycle, for the charge.

In particular, the temperature indicated as T_1 is the temperature at the suction of the fan; T_2 is the temperature reached at the outlet of the fan. These two temperatures, as expected, remain the same for all the charging process. The temperature T_3 is the temperature after the heat exchanger, and T_4 is the temperature reached at the outlet of the electric heater: as we can see, this is the maximum temperature of the cycle. Then, the temperature T_5 is the temperature at the outlet of the storage tank: as expected, close to the end of the charging phase, its value increases. Lastly, the temperature T_6 corresponds to the temperature at the outlet of the cycle, after the second passage in the heat exchanger.

To better understand the behaviour of the storage tank in these simulations, we decided to report in the following Figure 4.6 the temperature of the various layers, reached at the end of the simulation.

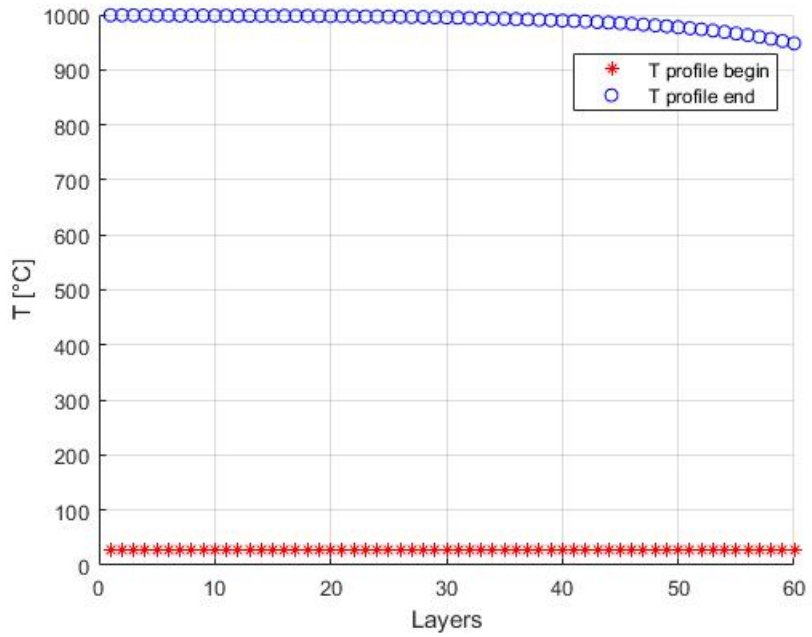

Figure 4.6: Temperature of the various layers at the beginning and at the end of the simulation, for the month of July.

Similar charts can be obtained considering the simulations for the month of December. In Figure 4.7 it is reported the temperature of the layers at the beginning and at the end of the simulation. In Figure we can instead see the temperature profile in the various points of the cycle for the last charging process. Again, T_1 is the temperature at the suction of the fan, T_2 is the temperature at the discharge of the fan; T_3 is the temperature at the outlet of the heat exchanger, T_4 the one at the exit of the electric heater. T_5 is the temperature at the exit of the storage and T_6 is the temperature after the heat exchanger, at the exit of the system.

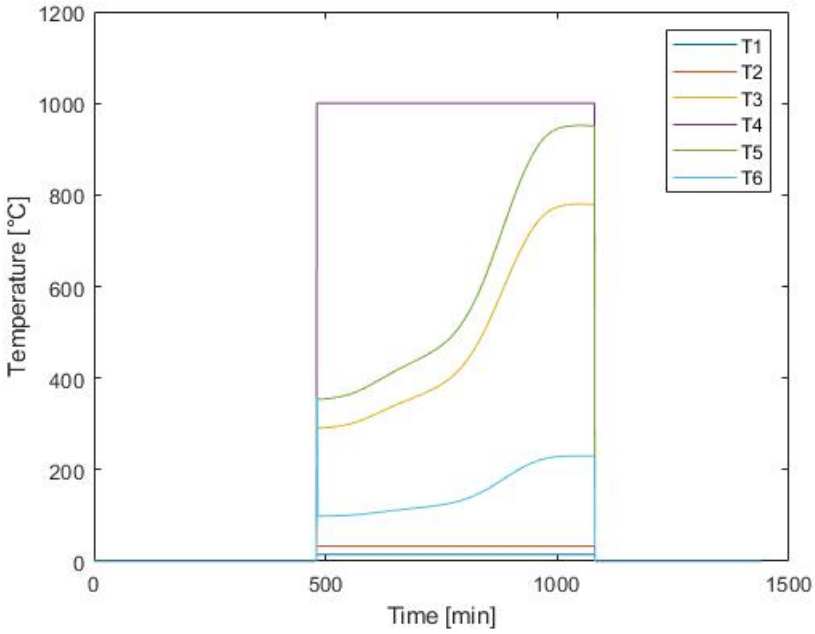

Figure 4.7: Temperatures of the points of the cycle during the charging phase.

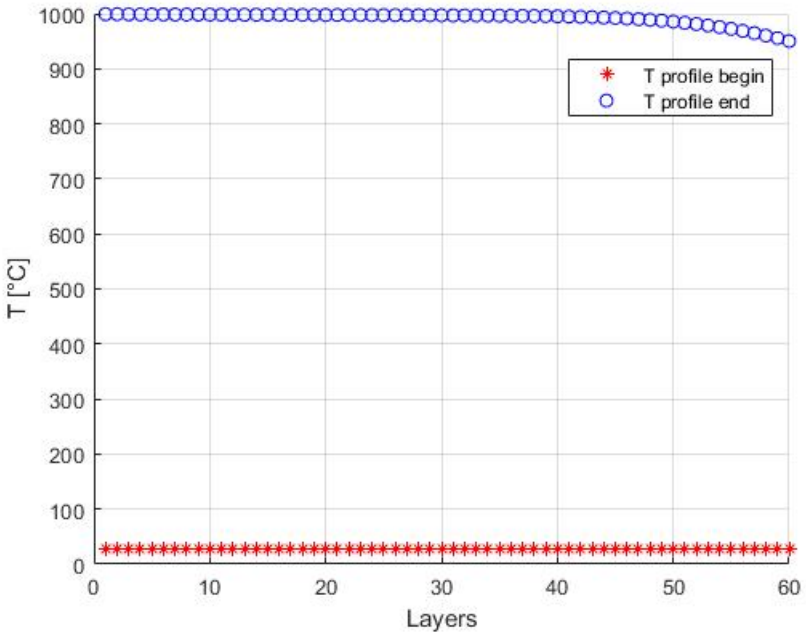

Figure 4.8: Temperature of the various layers at the beginning and at the end of the simulation, for the month of December.

In the Figure 4.8, we can see the temperature reached by the layers at the end of the charging process and the their temperature at the beginning of the simulation, that corresponds to the ambient external temperature.

At this point we want to perform some simulations accounting for the limit imposed by the correlation of Singh for the Nusselt number [26]. Thus, from the previous calculations we observed that the mass flow rate assumes very different values along the day, due to the different values of the power produced in the PV plant. For these simulations we decided to start considering the maximum flow rate observed along the charging phase and we consider to evaluate the minimum mass flow rate able to satisfy the limits imposed by Singh. Once the maximum and the minimum mass flow rates are obtained, we considered these as the limits in our model, for the charging. Moreover, starting from these values we evaluated the corresponding aspect ratio and height of the storage tank, that allows to work within the limits. In particular, given the maximum mass flow rate and the volume, we obtain the two limits in the aspect ratio, and we consider the maximum one as the minimum allowable aspect ratio in the determination of the minimum mass flow rate to be used in the charging process.

For the month of July, we observed that the maximum mass flow rate is equal to around 6.6 kg/s. Consequently, we obtain that the minimum mass flow rate to work within the limits of mass velocity is equal to 3.8 kg/s. Moreover, we obtain that the height of the storage tank is equal to 3.2 m. At this point, performing the simulation the volume obtained at the end is equal to 81 m^3. During the simulations performed, the mass flow rate used during the discharging phase was equal to the minimum mass flow rate calculated for the charge. We decided to report in the following Table 4.6. We can observe that the volume calculated in this simulation is lower with respect to the one obtained in the previous case. In fact, in this second simulation the limits associated to the correlation of Singh lead to a lower amount of energy that is stored in the device.

July		
$\mathbf{V_{final}}$	$[\mathbf{m^3}]$	81
$\mathbf{L}$	$[\mathbf{m}]$	3.2
$\mathbf{r_{c,fan}}$	$[-]$	1.4
$\mathbf{\dot{m}_{max}}$	$[\mathbf{kg/s}]$	6.6
$\mathbf{\dot{m}_{min}}$	$[\mathbf{kg/s}]$	3.8
$\mathbf{\dot{m}_{discharge}}$	$[\mathbf{kg/s}]$	3.9

Table 4.6: Results and parameters used in the month of July.

We proceed in the same way for the month of December. In particular, in this case we observed that the maximum mass flow rate reached during the charging phase is equal to 4 kg/s. Thus, the minimum admissible value for the mass flow rate is equal to 2.3 kg/s. For sake of clarity, in the Table 4.7 are reported the data used in the simulation for December.

December		
$\mathbf{V_{final}}$	$[\mathbf{m^3}]$	35
$\mathbf{L}$	$[\mathbf{m}]$	4
$\mathbf{r_{c,fan}}$	$[-]$	1.4
$\mathbf{\dot{m}_{max}}$	$[\mathbf{kg/s}]$	4
$\mathbf{\dot{m}_{min}}$	$[\mathbf{kg/s}]$	2.3
$\mathbf{\dot{m}_{discharge}}$	$[\mathbf{kg/s}]$	3.9

Table 4.7: Results and parameters used in the month of December.

Again, we can see that the volume obtained is lower with respect to the previous simulations. In fact, the charging process started only when the power produced by

the photovoltaic plant was high enough to give a sufficiently high mass flow rate, equal to the minimum value calculated considering the limits imposed by the usage of the correlation for the calculation of the Nuesselt number.

4.3 Store all the energy produced considering a constant power

Another way to evaluate the volume of the storage system is based on a charging phase characterized by a constant mass flow rate (and thus a constant power). In this case we are deriving from the electrical grid the energy required to perform the charging when the power generated in the PV plant is not high enough. Similarly, when there is a high production, in correspondence of the central hours of the day, the surplus is sell to the electrical grid. In this case, starting from the production curves of the photovoltaic plant, the duration of the charging phases is equal to the period in which the PV plant is generating power; when the production is null, the IT-ESS produce power during the discharge. During the month of July, the mass flow rate assumed during the charging phase is equal to $\dot{m}_{charge} = 3.4$ kg/s. During the discharge the mass flow rate is equal to $\dot{m}_{discharge} = 3.9$. Starting from these two values of mass velocities, the height of the storage system is evaluated considering the limits imposed by Singh [26]. The choice of the values of the mass flow rate for the charge of the storage tank is done considering the energy produced by the photovoltaic plant and the energy that is stored in the device: the mass flow rate considered gives allows to store a certain amount of energy that corresponds to the energy that is produced by the photovoltaic plant during its operation.

		July
$\mathbf{V_{final}}$	$[\mathbf{m^3}]$	76
$\mathbf{L}$	$[\mathbf{m}]$	3.7
$\mathbf{r_{c,fan}}$	$[-]$	1.4
$\mathbf{\dot{m}_{charge}}$	$[\mathbf{kg/s}]$	3.4
$\mathbf{\dot{m}_{discharge}}$	$[\mathbf{kg/s}]$	3.9

Table 4.8: Parameters and results obtained for the month of July.

In the Table 4.8, we reported the parameters adopted during the simulation and the volume obtained as results.

We proceeded in the same way, considering the month of December: in this case the values of the mass flow rates are $\dot{m}_{charge} = 2.4$ kg/s and $\dot{m}_{discharge} = 2.8$ kg/s. Consequently, the energy produced by the photovoltaic field is the same that is used to charge the storage device.

December		
$\mathbf{V_{final}}$	$[\mathbf{m^3}]$	24
$\mathbf{L}$	$[\mathbf{m}]$	1.9
$\mathbf{r_{c,fan}}$	$[-]$	1.4
$\mathbf{\dot{m}_{charge}}$	$[\mathbf{kg/s}]$	2.4
$\mathbf{\dot{m}_{discharge}}$	$[\mathbf{kg/s}]$	3.9

Table 4.9: Results of the simulation and parameters used for December.

Again, we reported the trends of the temperature in time for the two simulations performed:

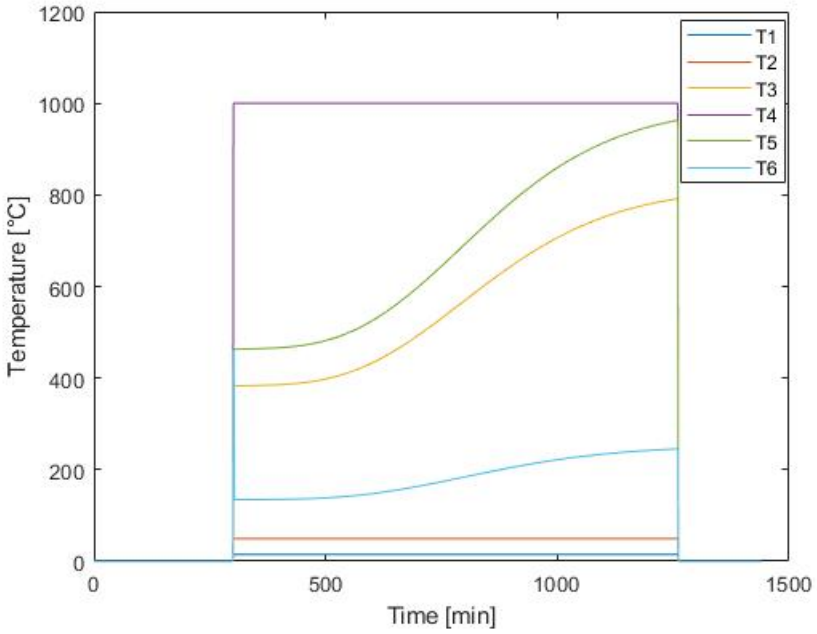

Figure 4.9: Temperatures of the various point during the simulation for July.

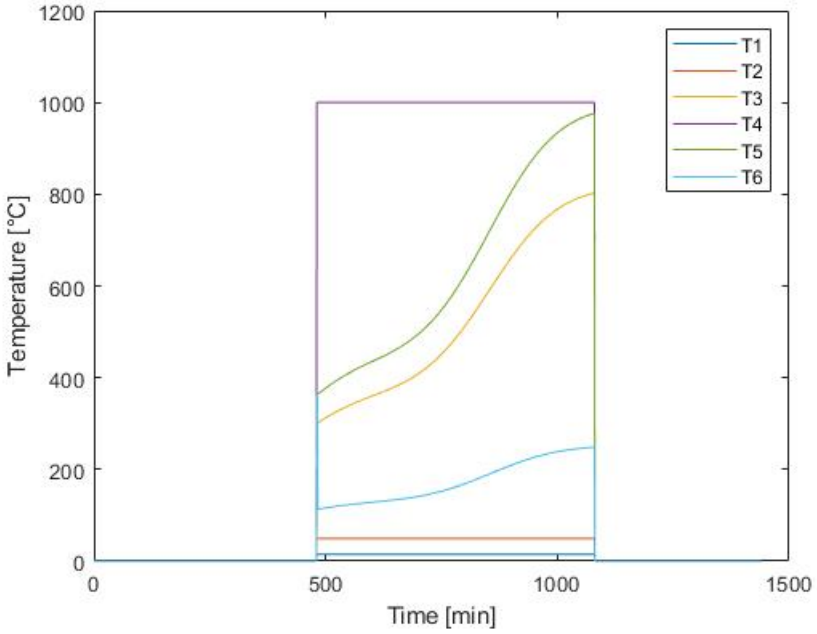

Figure 4.10: Temperatures of the various point during the simulation for December.

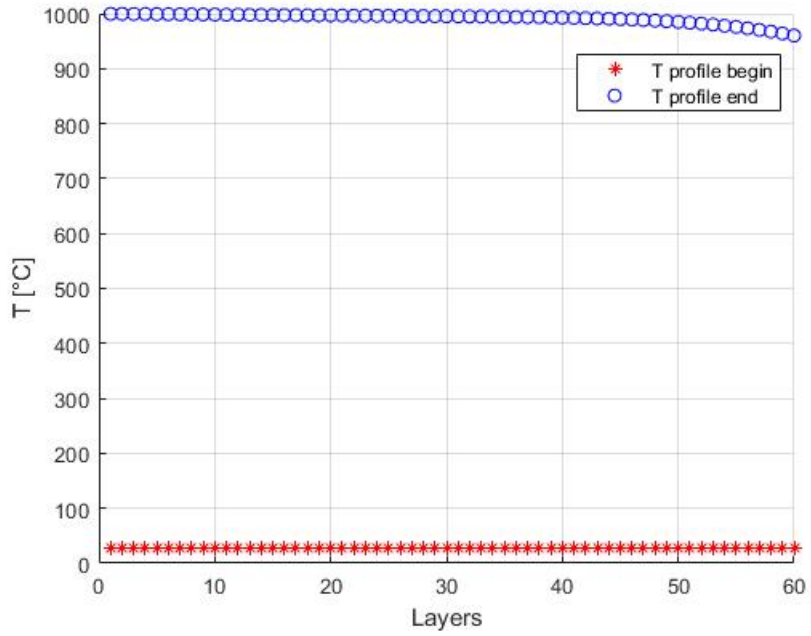

Figure 4.11: Temperatures of the layers for July.

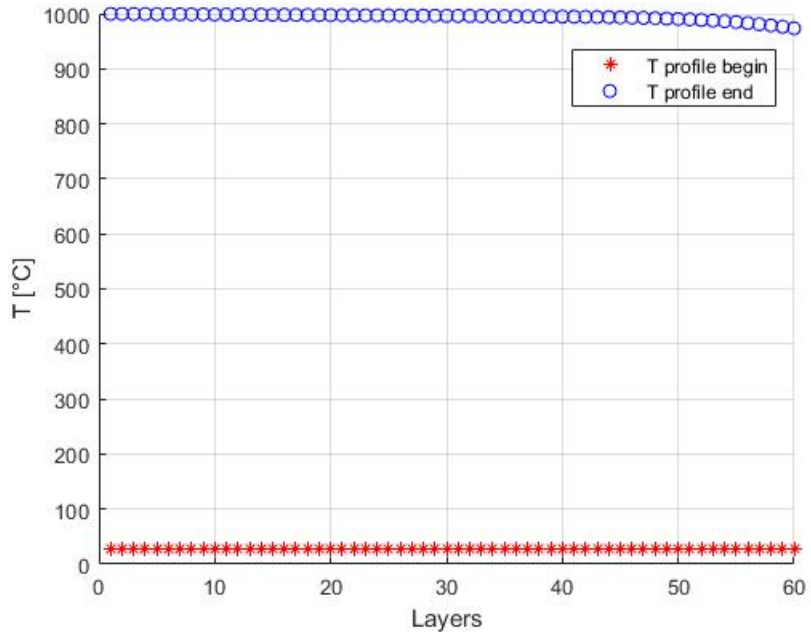

Figure 4.12: Temperatures of the layers for December.

Chapter 5

Costs and economical aspects

To properly understand the feasibility of the system proposed, it is fundamental to perform an economic analysis [21]. In particular, we are going to consider the equations presented in various previous works such as [21], [35] and derived from the book of Sinnott et al. [36].

For the fan, the cost is evaluated as:

$$C_{fan} = \exp\left(6.6547 + 0.97 \cdot \ln P_{fan}\right) \tag{5.1}$$

Where P_{fan} is the power absorbed by the fan during its functioning.

For the compressor and the turbine we have respectively:

$$C_{comp} = 39.5 \cdot \dot{m}_{air} \cdot \frac{r_c \cdot \ln r_c}{0.9 - \eta_{is,comp}} \tag{5.2}$$

$$C_{exp} = 266.3 \cdot \dot{m}_{air} \cdot \frac{\ln r_e \cdot (1 + \exp 0.036 \cdot T_{in} - 54.4)}{0.92 - \eta_{is,exp}} \tag{5.3}$$

In the previous expressions, r_c and r_e are the compression and the expansion ratios. T_{in} is the inlet temperature of the working fluid in the turbine and the isentropic efficiencies are designed as $\eta_{is,comp}$ and $\eta_{is,exp}$.

The cost of the storage tank is calculated as:

$$C_{storage} = 17400 + 79 \cdot W_{tank}^{0.85} \tag{5.4}$$

In the previous expression W_{tank} represents the mass of the storage tank.

The cost of the motor/generator is computed through the following correlation:

$$C_{mg} = 200000 \cdot \frac{[|P_{exp} - P_{comp}|_{max}]^{0.67}}{5000} \tag{5.5}$$

For the electric heater we have:

$$C_{eh} = 75000 \cdot P_{eh}^{0.9} \tag{5.6}$$

For the bed material, the cost is calculated as:

$$C_{bed} = 1500\$/ton \tag{5.7}$$

While the cost of the heat exchanger is determined considering the heat transfer area A_{hx}:

$$C_{hx} = 530000 \cdot \frac{A_{hx}^{0.9}}{3563} \tag{5.8}$$

Finally, the total cost is determined as the sum of the various components' costs:

$$C_{tot} = 1.1 \cdot \sum C_{device} \tag{5.9}$$

The multiplier factor in the previous expression is introduced to accounts for the various costs such as the operation and maintenance ones.

Moreover, we need to consider that the previous correlations were presented considering the value of the money in the year 2009. Thus, we have to introduce a factor that allows to determine the corresponding amount of money in the year 2023. This parameter, considering the variability of the value of the money in time, is assumed equal to 1.4.

The results are reported in the following Table 5.1. In particular, we denote as Simulation 1 the case in which we decided to follow the production curve, without accounting for the limits of the correlation of Singh; Simulation 2 refers to the case in which we accounted for the limits imposed by Singh. With Simulation 3 we are

referring to the simulations in which we considered a charging process characterized by a constant power.

		Cost [M$]	Cost [M€]
Simulation 1	**July**	2.78	2.58
Simulation 1	**December**	1.31	1.26
Simulation 2	**July**	1.96	1.82
Simulation 2	**December**	1.39	1.29
Simulation 3	**July**	1.46	1.39
Simulation 3	**December**	1.04	0.97

Table 5.1: Overall cost of the plant.

The results of the economic analysis demonstrated that the major costs are related to the purchase of the storage device and the storage material. This result is aligned to the results obtained in other works, such as the one of Benato et al. [21].

It is interesting to observe that the functioning of the system is scheduled in order to accumulate energy during the central hours of the day and to produce electricity when the power generated in the photovoltaic plant is null. Thus, it was decided to analyse which could be, in general terms, an hypothetical value of the economical return considering the gain derived from the discharging phase. To proceed in this way, the data related to the various trends of the price of the electricity are obtained consulting the website of Gestore Mercato Elettrico (`https://www.mercatoelettrico.org/it/default.aspx`), that is the reference Italian website for the electricity and energy markets. In this online platform, it is possible to analyse the daily and monthly trends of the prices of the electricity. For our analysis, we are going to consider the daily trend of the electricity's price, just for

the months of July and December, that are the two months considered in this work. For example, we can consider the daily profile of the 15th July, 2022. The profile is reported in the following Figure 5.1.

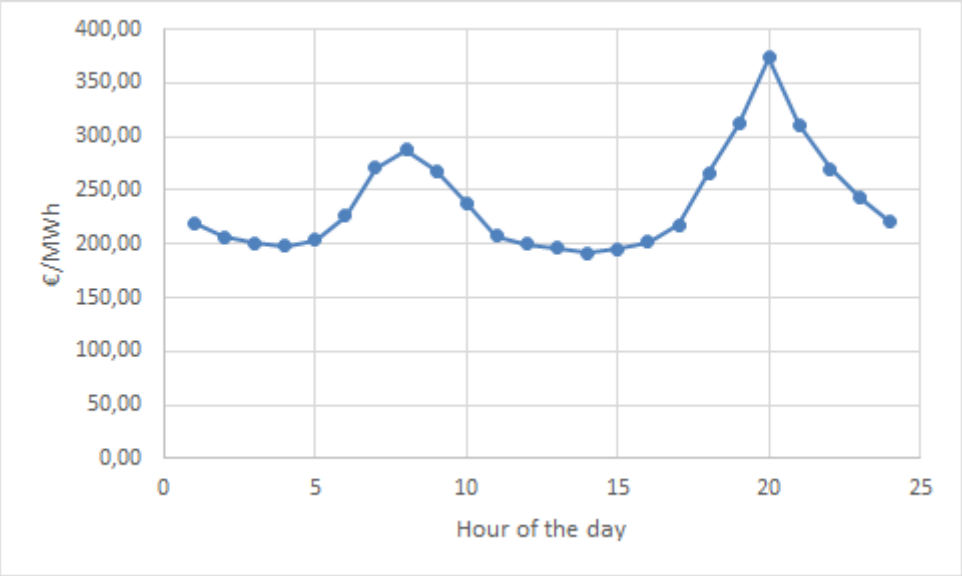

Figure 5.1: Hourly energy prices of the 15th July, 2022.

Considering the power production of the PV plant for the month of July, we can observe that the charging phase starts around the 5 in the morning and ends in the evening around the 21. The duration of the charging phase is of 16 hours, while the discharging phase last for 8 hours. Thus, considering an average price of the electricity in the hours in which the plant is generating electricity, and considering the average amount of energy produced by the IT-ESS during the discharging we can obtain the money earned. Considering the data previously reported in Figure 5.1, we observe that the average price in the discharging period is equal to 230.31 €/MWh. The electric generator installed is characterized by a power of 800 kW, and thus the energy produced in a typical day of July is around 6.4 MWh. Thus the earn for a day is equal to around 1438 €, and considering all the month of July it is equal to around 44600 €.

A similar analysis can be carried out for the month of December. From the website of Gestore Mercato Elettrico we can derive the data related to the prices (Figure 5.2).

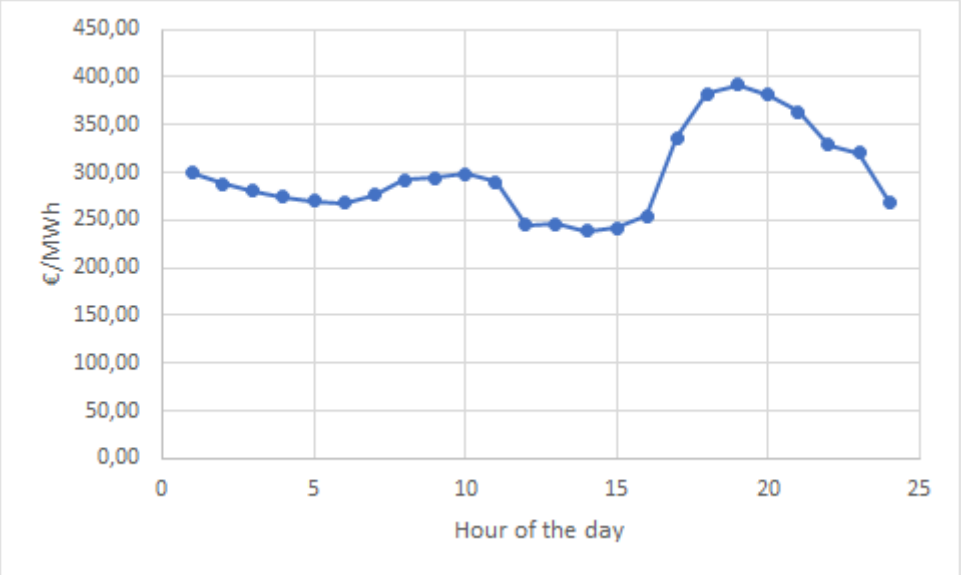

Figure 5.2: Hourly energy prices of the 11th December, 2022.

Again, from the photovoltaic production curves, we can observe that the charging phase starts around the 8 in the morning and ends around the 18 in the evening. The duration of the charging phase is of 10 hours, while the discharge lasts for around 14 hours. In this case, the average price of the electricity during the discharging process is equal to around 307 €/kWh. Thus the daily amount of money earned is equal to around 4298 €and the monthly one is equal to around 129000 €.

Averaging, we can assume a monthly earn for one month of operation of the plant of around 75000 €. Thus, along the year we can earn around 900000 €. Of course, in these calculations we are not accounting for the costs of ancillary services and the costs related to the operation and maintenance of the IT-ESS and the photovoltaic power plant. It is possible to evaluate some economical parameter such as the Simple

Pay Back time (SPB) or the Actualized Pay Back time (APB). The SPB can be defined as the number of years n for which the sum of the cash flow from the starting year to the year n gives a positive number (considering that the various costs are assumed as negative and the earns are assumed as positive). In the Actualized Pay Back time, we need to introduce the actualization factor a, that account for the value of the money in time. In this analysis, a cautionary value of the actualization factor is chosen $a = 5\%$.

In particular, considering the simulation with the highest costs of the system (Simulation 1, for the month of July), we reported in the following Table 5.2, the results for the SPB and the APB times.

Simulation 1 - July		
Cost	**[M €]**	2.58
SPB	**[year]**	2
APB	**[year]**	3

Table 5.2: SPB and APB for the first simulation, December.

We can observe that both the SPB and the APB assumes low values. This is a positive result, that demonstrates that the investment is good.

Anyway in this brief economical analysis we have not accounted for the various costs that regard the operation and the maintenance of the system, the cost for the replacement of old or damaged components and devices, and the various other costs related to the proper functioning of the entire system. Moreover, we have not included the costs of the photovoltaic power plant, that was assumed already existing in the various scenarios analysed. Thus, in future works, it is necessary to better and deeply investigate the economical aspects, to present a proper investment project that includes and accounts all the various elements that represents a cost during the functioning of the system.

Furthermore, for a more precise analysis of these systems, it is required to choose the proper management solutions and, thus, when to perform the discharging and evaluate the proper duration of this phase according to the daily curve of the electricity price. Anyway, it is possible to understand that the convenience of the storage and in general terms of the IT-ESS, is strongly related the to the price curve. Days in which the electricity price is characterized by a lower value during the day, in particular close to the central hours, in which the production of the photovoltaic plant (or another renewable power plant) is high, and when the price increases or is higher during the night, seems to be very suitable to adopt a storage system. As reference we report in the following Figure 5.3 the trend of a day in which the adoption of a storage system is particularly convenient.

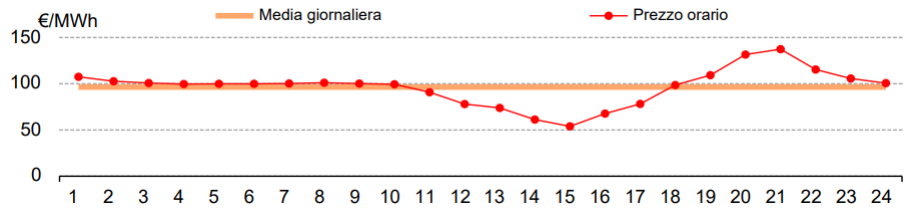

Figure 5.3: Hourly energy prices of the 2th September, 2023 (from the GME website).

In fact, as we can see, the profile is characterized by a lower price during the central hours of the day. Consequently, the storage allows to move the production and the selling of the electricity during the night. In this way, since the price is higher during the evening and in the early morning, the owner of the plant has an advantage in the implementation of an IT-ESS.

Chapter 6

Conclusions

In this Master's thesis I have investigated the various technologies available in the thermal energy storage field, considering both the ones already available and the in developing ones. In particular, the work was centered on the Integrated Thermal Energy Storage Systems, devices that constitute a promising technology for future works and projects in scenarios where our society is experiencing an important energy transition towards renewable sources. Moreover, we have studied the various models proposed along the years and used to describe the behaviour of the storage device, focusing in particular on the one proposed in the work of Benato et al. [24] and adopted in this work. We have analysed also the concept of Virtual Power Plant, that is fundamental to understand new possible management solutions of IT-ESS when coupled with the electrical grid.

After the literature review, the work analysed different strategies and how the volume of the storage device is affected by them. We have considered an IT-ESS coupled with a photovoltaic power plant, located in Sardinia. In particular, we have analysed a scenario in which the power used to feed the components of the system during the charging phase follows the production curve of the photovoltaic plant considered. In a second simulation, we have accounted for the important limits related to the correlation of Singh [26] for the calculation of the Nuesselt number, used in the description of the behaviour of the storage tank. The third

series of simulations was centered on a scenario in which the process of charging of the system was performed considering a constant mass flow rate, and thus a constant charging power.

At the end of the various simulations performed, to properly understand the feasibility of the solutions investigated in this work in economical terms, we evaluated the cost of the storage tank and the cost of the various other components that constitute the IT-ESS. In this phase we have used the various correlations proposed and utilized in various studies, and we have observed that the results obtained are aligned with the ones achieved in other works in which similar configurations have been investigated.

At the end of the work, we have understand that the Integrated Thermal Energy Storage System will play a central role in the energy transitions that we are going to face in the next years, and will find room in both the industrial and the residential sectors. The range of applicability of this technology can be enlarged considering not only the industrial world, but can also be part of stand-alone grids in remote areas. For these reasons, we have to investigate other aspects of this technology, in order to understand all its potentialities. In future works, other management solution will be investigated and analysed, in order to individuate which could be the best solution, considering the system coupled with other renewable sources and in different scenarios. Moreover, another important aspect that needs to be studied in future regards different materials for the packed bed of the storage device, to understand which is the role of the storage material on the behaviour of the system. In future studies, there is the also the need to study the system, with a special attention on the storage device, through a thermo-fluid-dynamic analysis and experimental tests. In this way, the energy storage device can be studied in a more complete way in order to better understand its thermodynamic behaviour.

Another possible solution that can be analysed and studied in future works is represented by a system in which we adopt a modular solution for the storage device: in other words, once the overall volume is individuated, it is possible to consider

different vessels characterized by a lower volume. In this cases, it is possible to decide which vessels are functioning in the same moment. This solution can be interesting in that situations in which the volumes required in different moment of the year are very different. In particular for the months with a greater production more vessels are charged at the same time, while in the months with a lower production, just one or few vessels are used to store the energy.

In addiction, the future researches on this topic can investigate the role of storage devices for cogenerative purposes, in which the systems are used to produce at the same time electricity and thermal energy. This will be extremely important in order to understand the incentives that can be obtained by these systems, in scenarios in which there will be a more stringent regulation on the production plant, defined, for example, through the White Certificates. Moreover, socio-economical aspects are crucial to properly understand which could be the role of the IT-ESS in future scenarios aimed to the decarbonization of the energy sector.

To properly understand the various scenarios, some economical analysis must be carried on. In future works it will be necessary to accounts for the various economical aspects to evaluate the feasibility of the investments and to evaluate also in which way the implementation of systems such as the ones described in this work can affect the electricity marked and consequently the prices and costs of the electrical energy.

List of Figures

List of Tables

Bibliography

[1] Seyed Ehsan Hosseini. "Transition away from fossil fuels toward renewables: lessons from Russia-Ukraine crisis". In: *Future Energy* 1.1 (2022), pp. 2–5.

[2] IEA. "World Energy Outlook 2022". In: *IEA* (2022). URL: https://www.iea.org/reports/world-energy-outlook-2022.

[3] Alberto Benato, Francesco De Vanna, and Anna Stoppato. "Levelling the photovoltaic power profile with the integrated energy storage system". In: *Energies* 15.24 (2022), p. 9521.

[4] Zakariya Dalala et al. "Increased renewable energy penetration in national electrical grids constraints and solutions". In: *Energy* 246 (2022), p. 123361.

[5] Enas Taha Sayed et al. "Renewable energy and energy storage systems". In: *Energies* 16.3 (2023), p. 1415.

[6] Abraham Alem Kebede et al. "A comprehensive review of stationary energy storage devices for large scale renewable energy sources grid integration". In: *Renewable and Sustainable Energy Reviews* 159 (2022), p. 112213.

[7] Alberto Benato and Anna Stoppato. "Pumped thermal electricity storage: a technology overview". In: *Thermal Science and Engineering Progress* 6 (2018), pp. 301–315.

[8] Mathew Aneke and Meihong Wang. "Energy storage technologies and real life applications–A state of the art review". In: *Applied Energy* 179 (2016), pp. 350–377.

[9] Francisco Dıaz-González et al. "A review of energy storage technologies for wind power applications". In: *Renewable and sustainable energy reviews* 16.4 (2012), pp. 2154–2171.

[10] Ioannis Hadjipaschalis, Andreas Poullikkas, and Venizelos Efthimiou. "Overview of current and future energy storage technologies for electric power applications". In: *Renewable and sustainable energy reviews* 13.6-7 (2009), pp. 1513–1522.

[11] Antoni Gil et al. "State of the art on high temperature thermal energy storage for power generation. Part 1—Concepts, materials and modellization". In: *Renewable and sustainable energy reviews* 14.1 (2010), pp. 31–55.

[12] Marc Medrano et al. "State of the art on high-temperature thermal energy storage for power generation. Part 2—Case studies". In: *Renewable and Sustainable Energy Reviews* 14.1 (2010), pp. 56–72.

[13] Olivier Dumont et al. "Carnot battery technology: A state-of-the-art review". In: *Journal of Energy Storage* 32 (2020), p. 101756.

[14] Tristan Desrues et al. "A thermal energy storage process for large scale electric applications". In: *Applied Thermal Engineering* 30.5 (2010), pp. 425–432.

[15] Alberto Benato. "Performance and cost evaluation of an innovative Pumped Thermal Electricity Storage power system". In: *Energy* 138 (2017), pp. 419–436.

[16] Alberto Benato and Anna Stoppato. "Energy and cost analysis of a new packed bed pumped thermal electricity storage unit". In: *Journal of Energy Resources Technology* 140.2 (2018).

[17] Mehmet Mercangöz et al. "Electrothermal energy storage with transcritical CO2 cycles". In: *Energy* 45.1 (2012), pp. 407–415.

[18] Matteo Morandin et al. "Conceptual design of a thermo-electrical energy storage system based on heat integration of thermodynamic cycles–Part A: Methodology and base case". In: *Energy* 45.1 (2012), pp. 375–385.

[19] Matteo Morandin et al. "Conceptual design of a thermo-electrical energy storage system based on heat integration of thermodynamic cycles–Part B: Alternative system configurations". In: *Energy* 45.1 (2012), pp. 386–396.

[20] Wolf-Dieter Steinmann. "The CHEST (Compressed Heat Energy STorage) concept for facility scale thermo mechanical energy storage". In: *Energy* 69 (2014), pp. 543–552.

[21] Alberto Benato and Anna Stoppato. "Energy and cost analysis of an Air Cycle used as prime mover of a Thermal Electricity Storage". In: *Journal of Energy Storage* 17 (2018), pp. 29–46.

[22] Joshua D McTigue, Alexander J White, and Christos N Markides. "Parametric studies and optimisation of pumped thermal electricity storage". In: *Applied Energy* 137 (2015), pp. 800–811.

[23] Alberto Benato and Anna Stoppato. "Integrated thermal electricity storage system: Energetic and cost performance". In: *Energy Conversion and Management* 197 (2019), p. 111833.

[24] Alberto Benato et al. "TES-PD: A Fast and Reliable Numerical Model to Predict the Performance of Thermal Reservoir for Electricity Energy Storage Units". In: *Fluids* 6.7 (2021), p. 256.

[25] J.R. Howell, R.B. Bannerot, and G.C. Vliet. *Solar-thermal Energy Systems: Analysis and Design*. McGraw-Hill, 1982. ISBN: 9780070306035. URL: `https://books.google.it/books?id=v-RSAAAAMAAJ`.

[26] Ranjit Singh, RP Saini, and JS Saini. "Nusselt number and friction factor correlations for packed bed solar energy storage system having large sized elements of different shapes". In: *Solar energy* 80.7 (2006), pp. 760–771.

[27] To EW Schumann. "Heat transfer: a liquid flowing through a porous prism". In: *Journal of the Franklin Institute* 208.3 (1929), pp. 405–416.

[28] Alexander White, Joshua McTigue, and Christos Markides. "Wave propagation and thermodynamic losses in packed-bed thermal reservoirs for energy storage". In: *Applied Energy* 130 (2014), pp. 648–657.

[29] RE Hicks. "Pressure drop in packed beds of spheres". In: *Industrial & engineering chemistry fundamentals* 9.3 (1970), pp. 500–502.

[30] N Wakao and T Funazkri. "Effect of fluid dispersion coefficients on particle-to-fluid mass transfer coefficients in packed beds: correlation of Sherwood numbers". In: *Chemical Engineering Science* 33.10 (1978), pp. 1375–1384.

[31] Hossein Mohammadi Rouzbahani, Hadis Karimipour, and Lei Lei. "A review on virtual power plant for energy management". In: *Sustainable energy technologies and assessments* 47 (2021), p. 101370.

[32] Kaile Zhou, Shanlin Yang, and Zhen Shao. "Energy internet: the business perspective". In: *Applied energy* 178 (2016), pp. 212–222.

[33] Carmen Ramos et al. "Small-scale renewable power technologies are an alternative to reach a sustainable economic growth: evidence from Spain". In: *Energy* 167 (2019), pp. 13–25.

[34] Bjarne Steffen. "Estimating the cost of capital for renewable energy projects". In: *Energy Economics* 88 (2020), p. 104783.

[35] Alberto Benato and Anna Stoppato. "Heat transfer fluid and material selection for an innovative Pumped Thermal Electricity Storage system". In: *Energy* 147 (2018), pp. 155–168.

[36] R. Sinnott and G. Towler. *Chemical engineering design: SI Edition*. Butterworth-Heinemann, 2009.